

1 **Diagnosing Hydrological Process Controls in Streamflow Generation and Variability in a**
2 **Glacierized Alpine Headwater Basin**

3
4 Caroline Aubry-Wake¹, Dhiraj Pradhananga^{1,2}, John W. Pomeroy¹

5 ¹Centre for Hydrology, University of Saskatchewan, Canmore, Canada

6 ²Tribhuvan University, Kathmandu, Nepal

7
8 **Corresponding Author:** Caroline Aubry-Wake, caroline.aubrywake@gmail.com, 116A - 1151 Sidney
9 Street, Canmore, AB, T1W 3G1

10
11 **Abstract:**

12 Mountain glacierized headwaters are currently witnessing a transient shift in their hydrological and
13 glaciological systems in response to rapid climate change. To characterize these changes, a robust
14 understanding of the hydrological processes operating in the basin and their interactions is needed. Such
15 an investigation was undertaken in the Peyto Glacier Research Basin, Canadian Rockies over 32 years
16 (1988-2020). A distributed, physically based, uncalibrated glacier hydrology model was developed using
17 the modular, object-oriented Cold Region Hydrological Modelling Platform to simulate both on and off-
18 glacier high mountain processes and streamflow generation. The hydrological processes that generate
19 streamflow from this alpine basin are characterized by substantial inter-annual variability over the 32
20 years. Snowmelt runoff always provided the largest fraction of annual streamflow (44% to 89%), with
21 smaller fractional contributions occurring in higher streamflow years. Ice melt runoff provided 10% to 45%
22 of annual streamflow volume, with higher fractions associated with higher flow years. Both rainfall and
23 firn melt runoff contributed less than 13% of annual streamflow. Years with high streamflow were on
24 average 1.43 °C warmer than low streamflow years, and higher streamflow years had lower seasonal snow
25 accumulation, earlier snowmelt and higher summer rainfall than years with lower streamflow. Greater
26 ice exposure in warmer, low snowfall (high rainfall) years led to greater streamflow generation. The
27 understanding gained here provides insight into how future climate and increased meteorological
28 variability may impact glacier meltwater contributions to streamflow and downstream water availability
29 as alpine glaciers continue to retreat.

30
31 **Keywords:** Glacio-hydrological modelling; streamflow; mountain hydrology; cold regions hydrology;
32 Canadian Rockies; CRHM.

33 1. INTRODUCTION

34 Glacierized mountain basins provide water to almost one-third of the world's population (Beniston, 2003),
35 but mountain glaciers are retreating quickly and expected to lose 30-80% of their volume by the end of
36 the century (Huss *et al.*, 2017). Their retreat is impacting water resources across the globe, as glaciers
37 have a strong influence on their basin hydrological regime due to their capacity to store water on seasonal
38 to decadal time scales (Jansson *et al.*, 2003). By storing water as snow and ice during cold and wet periods,
39 and releasing it in dry and hot periods, glaciers can modulate streamflow variability via a compensatory
40 effect occurring both at a decadal, seasonal and even weekly timescale (Jansson *et al.*, 2003). For instance,
41 Pradhananga and Pomeroy (2022a) found that increasing glacier ice melt compensated for declining
42 precipitation and snowmelt in two Canadian Rockies glacierized catchments, resulting in increased
43 discharge since the 1960s, showcasing the decadal capacity of the glacier compensation effect. On a
44 weekly timescale, Van Tiel *et al.* (2021) found that glacier and snow melt in glacierized basins with a 5-
45 15% glacier cover could compensate for precipitation deficits and increased evapotranspiration in the
46 European Alps. Even though a glacier coverage of roughly 40% has been suggested to minimize inter-
47 annual variability (and maximize the glacier compensation effect) (Fountain and Tangborn, 1985; Chen
48 and Ohmura, 1990; Jansson *et al.*, 2003), a recent analysis of streamflow in glacierized basins worldwide
49 was not able to define a universal relationship between glacier coverage and streamflow variability and
50 instead hinted at the range of hydrological processes that can complicate the relationship (van Tiel *et al.*,
51 2020a). Snow and ice melt in glacierized basins can also overcompensate for weather conditions and cause
52 an increase in streamflow variability (van Tiel *et al.*, 2020a, 2021). In the Canadian Rockies, Hopkinson and
53 Young (1998) showed that glacier meltwater does not always effectively augment streamflow during low
54 flow, dry years. This is in accordance with research showing that during cold years, glacier meltwater can
55 be significantly reduced and induce “glacier melt drought” (Van Loon *et al.*, 2015). For tropical glaciers,
56 glacier meltwater can be the driver of variability in streamflow from hourly to annual timescales (Saberi
57 *et al.*, 2019). These results hint at the complex interactions amongst glacier melt, streamflow generation
58 and seasonal meteorological conditions.

59
60 The role alpine glaciers play in modulating inter-annual flow variability is further complicated by their
61 recent and predicted retreat (Radic and Hock, 2014; Shannon *et al.*, 2019; Hugonnet *et al.*, 2021). As
62 currently glaciated mountain headwater basins transition from glacier melt runoff to more rainfall-runoff
63 and snowmelt runoff, they will shift towards a more variable hydrological regimes linked with the
64 decreased capacity of glaciers to provide reliable flow compensation. This shift is already noticeable in the
65 Alps and Pyrenees, where runoff volume is more tightly controlled by seasonal snow accumulation and
66 runoff peaks are associated with snowmelt and the occurrence of large rainfall volumes than with glacier
67 melt (Milner *et al.*, 2017). López-Moreno *et al.* (2020) have shown that as snowmelt-dominated alpine
68 basins warm, their streamflow regimes decouple from snow hydrology regimes, suggesting a progression
69 from glacier-modulated to seasonal snowpack-modulated to rainfall-modulated hydrological regime.
70 There is increasing interannual variability along this progression as hydrological memory times shorten
71 from glaciers to seasonal snowpacks to rainfall (Milner *et al.*, 2017). Combining this decrease in the
72 interannual buffering capacity of glacier runoff with an expected increase in extreme weather and
73 hydrological events such as increased heavy precipitation and droughts (Seneviratne *et al.*, 2012),

74 significant changes are expected to occur to the hydrology of mountain glacierized headwater basins
75 around the world.

76

77 Analyzing the influence of glacier runoff on headwater basin streamflow is further complicated by the
78 variety of approaches used to define glacier contributions to streamflow. Within the range of
79 methodologies, glacio-hydrological modelling is the most used (Frenierre *et al.*, 2013). Glacio-hydrological
80 models can be used to increase the understanding of the observed processes in a basin (Verbunt *et al.*,
81 2003), and can help diagnose the relationship between the different hydrological processes. These glacio-
82 hydrological models are typically adapted from models with either a glaciological or hydrological
83 background, depending on the intended use. Glaciological models typically focus on the ice processes, for
84 example, the representation of ice dynamics (Huss *et al.*, 2010; Clarke *et al.*, 2015) or surface mass balance
85 (Hock and Holmgren, 2005), but either ignore or simplify the other hydrological and cryospheric processes
86 (Immerzeel *et al.*, 2010). Hydrological models typically simplify the glacier-specific processes, such as
87 neglecting ice dynamics (Comeau *et al.*, 2009; Jost *et al.*, 2012), but can have more sophisticated
88 representations of the terrestrial hydrological cycle. Both model approaches often use a conceptual
89 approach to parametrize surface melt, using statistical associations to infer mass and energy fluxes, such
90 as the calibrated temperature-index, degree-day and melt models (Hock, 2003; Finger *et al.*, 2011; Fatichi
91 *et al.*, 2014; Ragettli *et al.*, 2016; Chernos *et al.*, 2020). While this makes them easier to apply in areas with
92 incomplete forcing data, a typical issue for mountain environments, it also makes them more prone to
93 problems such as equifinality (Beven, 2006), which can be reduced by using multi-criteria calibration
94 procedures (Jost *et al.*, 2012; Pellicciotti *et al.*, 2012; Hanzer *et al.*, 2016; van Tiel *et al.*, 2020b). A further
95 concern with these calibrated empirical modelling approaches is their transferability in time (Hock, 1999),
96 especially their ability to simulate conditions outside of the conditions encountered in the calibration
97 period (Duethmann *et al.*, 2020). Some glacio-hydrological model calibration strategies involve using
98 unusual years, such as the hot and dry year of 2003 in the European Alps, to assess model performance
99 under extreme events (Koboltschnig and Schöner, 2011). However, with rapidly changing meteorological
100 conditions and land cover, past conditions are not likely to represent future melt and hydrological events
101 in glacierized alpine basins. Empirically calibrated glacio-hydrological models also increase predictive
102 uncertainty as they are not consistent with the current understanding of glacio-hydrological physical
103 processes. Since shortwave radiation rather than air temperature is the main driver of glacier melt, and
104 snow redistribution is an important control on snow accumulation, the lack of a physical basis for these
105 models is scientifically unsatisfying in that process diagnoses are not possible and predictive uncertainty
106 is high because they are calibrated to past climate and glacier conditions. Models with a more complete
107 range of representations of glacio-hydrological processes do exist (Naz *et al.*, 2014; Frans *et al.*, 2018;
108 Pradhananga and Pomeroy, 2022b, 2022a), but these are still not widely used despite the uptake of
109 models of similar complexity for cold regions hydrological applications (Wheater *et al.*, 2022). To
110 investigate the inter-annual variability in the hydrology of a glacierized headwater basin and to diagnose
111 the hydrological processes governing this variability requires a physically based model, with
112 representations of both on and off-glacier biophysical processes. Glacierized basins are complex systems,
113 with several hydrological processes on and off the glacier such as snow redistribution, accumulation and
114 ablation, glacier processes, infiltration into seasonally frozen soils, groundwater storage and flow, frozen
115 ground, evapotranspiration and a dynamic land cover. These interconnected processes, driven by complex

116 physical feedbacks, should be included in hydrological assessments of glacierized headwater basins to
117 gain a robust understanding of the sources of hydrological variability occurring in these basins.

118
119 The objective of this paper is to assess and characterize the inter-annual hydrological variability of a long-
120 studied alpine glacierized headwater basin in the Canadian Rockies using observations and a physically
121 based glacio-hydrological model, including the full range of processes occurring both on and off the
122 glacier. Specifically, this study investigates the influences of meteorological conditions on hydrological
123 processes, meltwater production, runoff and streamflow variability by addressing the following questions:

- 124
125 1) What trends are evident in the hydrometeorological behaviour of the basin in the recent decades?
126 2) How do runoff source and streamflow regime vary with seasonal hydrometeorological
127 conditions?
128 3) How do meteorological conditions, snow dynamics and sources of runoff vary between high and
129 low streamflow years?

130

131 **2. DATA AND METHODS**

132 **2.1. Study site and available data**

133 This study focused on the Peyto Glacier Research Basin (PGRB, Fig. 1), a small glacierized headwater basin
134 in the Canadian Rockies.. Peyto Glacier, the northernmost outlet glacier of the Wapta Icefield, ranges
135 between 2100-3190 m.a.s.l. and had an area of 10.2 km² in 2016, with a drainage basin of 19.3 km² as
136 defined by a stream gauge installed by the University of Saskatchewan's Centre for Hydrology in 2012.
137 Peyto Glacier is one of the few well-monitored glaciers in western Canada, and has one of the longest
138 time series of measurements in the world, with mass balance observed yearly since 1965, and glacier
139 extent measured since 1896 (Demuth *et al.*, 2006). The rest of the basin is composed of moraine deposits,
140 talus fields, and exposed bedrock, including cliffs (Fig 1b).

141

142 *[Figure 1 near here]*

143

144 The meteorological data used for model forcing and evaluation in this study have been described in detail
145 in Pradhananga *et al.* (2021) and by Pradhananga and Pomeroy (2022b), but a summary is provided here.
146 An automated weather station (AWS), Peyto Main Old, has recorded sub-hourly to hourly air temperature,
147 relative humidity, incoming solar radiation, incoming longwave and wind speed since 1987, at an altitude
148 of 2240 m.a.s.l. Due to the remote location and harsh conditions found in the basin, gaps are present in
149 the data since the installation. The record from Peyto Main Old between 1987 and 2018 is 94% complete,
150 with few gaps in the 2018 to 2020 period. When data gaps were less than or equal to four hours, they
151 were filled with either linear interpolation, and when gaps were more than 4 hours, they were filled with
152 data from nearby stations using monthly linear regression such as from the new Peyto main station,
153 installed in 2013 adjacent to the Peyto Main Old AWS. When nearby stations were not available to fill the
154 missing data, the gaps were infilled using ERA-Interim data, which were bias-corrected and downscaled
155 to the station location using a quantile mapping technique with monthly calibrated parameters from in-
156 situ data (Dee *et al.*, 2011).

157
158 Precipitation for the PGRB for 1987-2020 was obtained from the ERA-Interim reanalysis product. The ERA-
159 Interim precipitation data were also corrected using the quantile mapping technique using monthly
160 calibrated factors, but the in-situ data used to derive these factors were obtained from the Alberta
161 Environment Bow Summit weather station, located 5 km down valley at an elevation of 2030 m.a.s.l., from
162 which a reliable, sheltered-environment hourly precipitation record is available since 2008.

163
164 Glaciological data are available both as elevation-band averaged summer and winter point mass balance
165 for the 1993-1995 period (Dyurgerov, 2002) and as individual stake point-balance measurements for the
166 2003-2017 years. Additionally, glacier surface elevation change was measured intermittently using an
167 ultrasonic depth sensor on the on-ice AWS for the 2011-2020 period, and surface lowering associated
168 with ice melt has been transformed to surface melt water equivalent using an ice density of 0.9 kg m^{-3}
169 (Benn and Evans, 2010).

170
171 In 2013, an ultrasonic depth sensor (SR50) was installed 1 km below the glacier snout at a bedrock
172 constriction, which acts as a natural notch, providing a reliable control on the relation between
173 streamflow and stage discharge. Starting in early fall 2017, salt dilution measurements were performed to
174 build a rating curve to relate the water level at the sonic depth sensor to discharge (Sentlinger *et al.*,
175 2019; Pradhananga *et al.*, 2021, Aubry-Wake *et al.*, in prep.). Manual stream width measurements
176 provided values ranging between 8 and 13 m, and a mixing reach of length of 420 m was set based on the
177 local geomorphology to constrain the salt measurement between two naturally occurring bedrock
178 notches constricting the flow. A total of 105 salt dilution measurements were conducted between 2017
179 and 2019 and processed in the Fathom Scientific Salt Portal platform, an online post-processing platform
180 for salt dilution measurements (salt.fathomsscientific.com). Of these 105 measurements, 46 were
181 determined to be anomalous due to incomplete mixing associated with the choice of location for the
182 conductivity probe, localized snowmelt runoff, and the high background noise in electrical conductivity.
183 The resulting rating curve, based on 59 measurements with an average uncertainty of 12%, is a power law
184 with an inflection point at depth of 0.75 m due to a change in the slope of the bedrock notch walls. The
185 rating curve is stable over the 2017-2019 observations, as expected from the bedrock notch controls on
186 streamflow over the salt dilution mixing reach. This stability suggests it is appropriate to use the same
187 rating curve for the entire 2013-2020 melt seasons. Streamflow observations are only possible when the
188 melt channel is sufficiently free of snow that the SR50 sensor can measure open water, which results in
189 streamflow measurement available from mid-May/early June to late September/mid-October.

190 191 **2.2. Modelling approach**

192 The Cold Regions Hydrological Modelling Platform (CRHM, Pomeroy *et al.*, 2007; Pradhananga and
193 Pomeroy, 2022b) was used to investigate the hydrological processes and inter-annual variability in the
194 PGRB. The model was run at an hourly resolution for the period 1987-2020, with the first year acting as a
195 spin-up period. The modelled period covers 32 continuous hydrological years (October 1st – September
196 31st), starting in October 1988 and ending in September 2020. The model outputs were aggregated into
197 daily values for the analysis. The analysis period was dictated by the availability of in-situ meteorological
198 information in the PGRB (Pradhananga *et al.*, 2021).

199
200 CRHM is a process-based, flexible, modular hydrological modelling platform. The user can select processes
201 from an extensive library to assemble a custom hydrological model suited to the complexity, knowledge
202 and available data from the study environment. CRHM has been extensively used in mountains in the
203 recent years (DeBeer and Pomeroy, 2009; MacDonald *et al.*, 2010; Fang *et al.*, 2013; Rasouli *et al.*, 2014;
204 Zhou *et al.*, 2014; Krogh *et al.*, 2015; López-Moreno *et al.*, 2017) with applications over different terrain
205 and climate and at different spatial scales. A glacier module has recently been developed to represent ice
206 and firn melt and mass balance using an energy balance approach (Pradhananga and Pomeroy, 2022b).
207 This model is selected amongst other models because it has spatially distributed energy balance forcing
208 and a set of modules that represent hydrological processes suitable for the PGRB including blowing snow
209 transport and sublimation, complex terrain wind flow, avalanching, infiltration into seasonally frozen soils
210 and evaporation from soils, vegetation and open water and surface and sub-surface runoff generation.

211
212 The modelling work presented here used the CRHM model development from Pradhananga and Pomeroy
213 (2022b) and the PGRB data processing of Pradhananga *et al.* (2021). However, it differed substantially
214 from the CRHM application to the PGRB by Pradhananga and Pomeroy (2022a, 2022b). The study used in-
215 situ forcing data instead of reanalysis data (except precipitation) and simulated different time periods
216 (1989-2020 in this case and 2013-2018 and 1967-1977 in Pradhananga and Pomeroy, 2022a). In addition,
217 the current application used a different energy-balance parametrization for the glacier ice melt at an
218 hourly timestep as described in section 2.2.2.3, while Pradhananga and Pomeroy (2022a) used a daily
219 formulation without parametrization of sub-debris melt. The model spatial discretization and
220 parametrization was performed independently from these previous studies and resulted in a different
221 parametrization. For example, Pradhananga and Pomeroy (2022a) had a spatial discretization with 65
222 HRUs, and only 37 are used in this study. In addition, the research goals of this study, specifically to
223 investigate processes resulting in streamflow variability in the PGRB, were different from those of
224 Pradhananga and Pomeroy (2022a, 2022b), and therefore resulted in a different analysis methodology.

225

226 **2.2.1. Spatial discretization**

227 In CRHM, the mass and energy balance are calculated at the scale of hydrological response units (HRUs),
228 a spatial unit over which the mass and energy balance is assumed to be spatially uniform. HRUs are
229 defined as regions with similar hydrological characteristics and common parameters, based on
230 topographic, drainage, vegetation, soils, and hydrometeorological properties. Here, glacier properties
231 were also included in discretizing the basin into HRUs. PGRB was divided into 36 HRUs that represent the
232 glacier retreat over the 1987-2017 period, as well as the firn line retreat and major land cover types such
233 as moraine, talus, ice-cored moraine, and cliffs (Fig. 1b, c). The changing land cover types were manually
234 defined using a combination of Landsat imageries for glacier and firn, and field observations for cliffs,
235 moraines and talus characterization. The ice-cored moraine area was defined following Hopkinson *et al.*
236 (2012). For each HRU, parameters such as slope, aspect, elevation, and terrain view factor were then
237 defined using the SRTM digital elevation model. The resulting HRUs, with associated cover-type, can be
238 seen in Fig. 1b-c, and the elevation, slope, angle aspect and cover-type of each HRU can be found in table
239 A1.

240

241 **2.2.2. Physical processes representation and parametrization in CRHM-glacier**

242 A purpose-built model representing the hydrological processes observed in the PGRB was designed by
243 selecting modules in the CRHM modelling library. Parameters for each module have a physical meaning
244 and can be obtained from field site or remote sensing observations. When parameters specific to the site
245 are unavailable, parameters are obtained following the abduction approach (Pomeroy *et al.*, 2013),
246 meaning they are transferred from studies in similar environments or obtained from compatible
247 hydrological environments described in the scientific literature. In other words, as this CRHM model is
248 based on physical processes, it does not require a parameter calibration scheme based on streamflow
249 observations. The CRHM process representation and parameter estimation approaches are described
250 below.

251

252 **2.2.2.1. Distributing meteorological inputs**

253 The CRHM model created for PGRB distributes the forcing meteorology, namely observations of air
254 temperature, relative humidity, wind, incoming shortwave and longwave radiations and wind speed,
255 spatially and temporally over the basin. The air temperature lapse rate was defined for monthly values,
256 ranging from -0.57 to - 0.81 °C per 100 m, obtained from three on-ice AWS located on the glacier toe, near
257 the equilibrium line, and in the accumulation area for the years 2010-2013 as in Pradhananga and
258 Pomeroy (2022b) (Figure 1a). The shallowest temperature elevation lapse rates (slower decrease in
259 temperature with elevation gain) occurred in July and August, with generally steeper temperature
260 elevation lapse rates (faster decrease in temperature with elevation) occurring in Fall and Spring. Monthly
261 values for the temperature lapse rates were fixed throughout the simulation period (i.e., all Januaries had
262 the same lapse rate). The precipitation elevation gradient was derived from the end-of-winter SWE point
263 measurement over the glacier area for two 3-year periods (2003-2005 and 2014-2016) and so integrates
264 the winter snow accumulation season. The same precipitation gradient was used for all seasons, as there
265 was no information available to estimate a seasonally varying gradient for this basin. Precipitation phase
266 partitioning was calculated using the psychrometric energy balance of a falling hydrometeor based on air
267 temperature and relative humidity (Harder and Pomeroy, 2013). Wind flow acceleration and deceleration
268 over PGRB's complex terrain, an important component to capture blowing snow processes and turbulent
269 transfer calculations, were simulated following a linearized turbulence model (Walmsley *et al.*, 1986).
270 Radiation was adjusted for self-shading and slope-aspect following the formulations of Garnier and
271 Ohmura (1970), but it was not corrected for shading from surrounding terrain.

272

273 **2.2.2.2. Snow redistribution**

274 CRHM simulates winter snow redistribution from blowing snow with the Prairie Blowing Snow Model
275 module (Pomeroy *et al.*, 1993; Pomeroy and Li, 2000), which was initially developed in the Canadian
276 Prairies but has since then been parameterized for alpine and arctic tundra (Pomeroy *et al.*, 1997),
277 mountainous subarctic terrain (MacDonald *et al.*, 2009) and mountain ridges (MacDonald *et al.*, 2010).
278 The blowing snow sequence follows the dominating westerly wind patterns, from the peaks on the
279 continental divide, east to the glacier toe. Blowing snow redistribution requires a terrain roughness
280 specification, which in the absence of vegetation represents surface undulations and barriers. This was

281 set to between 0.5 and 3 m based on cover type and field observations. Fetch distance was obtained from
282 the length of the HRU in the predominating wind direction.

283
284 In high mountain environments, avalanches can redistribute an important part of the snow accumulation
285 (Shea *et al.*, 2015). Avalanches are highly dependent on slope, snow accumulation and meteorological
286 factors (Schweizer *et al.*, 2008; Freudiger *et al.*, 2017). CHRMs use the *SnowSlide* model as a module to
287 represent avalanche redistribution of snow, based on a threshold snow holding depth and slope
288 (Bernhardt and Schulz, 2010; Bernhardt *et al.*, 2012). The minimum threshold depth was set to 500 mm
289 w.e. for most HRU, with a holding capacity of 50 mm w.e. for the HRU with a surface slope angle above
290 30°, as steep terrain is more likely to avalanche frequently (McClung and Schaerer, 2006).

291 292 **2.2.2.3. Snow and ice melt**

293 Snowmelt on- and off-glacier in CRHM is calculated with the SNOBAL module (Marks *et al.*, 1999). This
294 module approximates the snowpack as being composed of two layers: a surface-active layer of fixed
295 thickness and a lower layer representing the remaining snowpack. The module solves for the temperature,
296 liquid water content and the specific mass of each layer for each time step. The point energy balance of
297 the snowpack is expressed as in the following:

$$298 \quad Q_m = Q^* + Q_H + Q_E + Q_G + Q_P - \frac{dU}{dt} \quad (\text{Eq. 1})$$

299
300 where Q_m is the energy available for snowmelt, Q^* is the net radiation composed of both shortwave and
301 longwave components, Q_H , Q_E and Q_G are the sensible, latent and ground heat fluxes, respectively, Q_P is
302 the energy added to the snowpack by precipitation, all in W m^{-2} , and U is the internal energy of the
303 snowpack in Joules. The snow albedo decay function (Essery and Etchevers, 2004) requires a maximum
304 (fresh snow) and a minimum (bare ground) albedo, which in this case was set to 0.85 and 0.17 from
305 regional observations. For glacier and firn, the albedo was set to 0.3 and 0.5 respectively. The snowmelt
306 module was given a surface snow roughness of 0.0055 m based on the observations of Munro (1989) from
307 Peyto Glacier. Turbulent transfer energy fluxes in the module are calculated using a bulk transfer
308 formulation with the Monin-Obukhov stability corrections.

309
310
311 Once the snow is melted, glacier ice melt is calculated using a single layer energy balance model, with the
312 residual of the radiation and turbulent fluxes resulting in energy available for melt (Hock, 2005). The
313 model distinguishes between firn and ice cover for albedo, roughness length and density. The energy
314 balance formulation for the ice and firn melt uses turbulent energy fluxes calculated following the
315 katabatic parametrization of the bulk transfer method as described by Grisogono and Oerlemans (2001)
316 and tested at Peyto Glacier by Munro (2004). This is an advance over the simpler daily ice melt energy
317 balance parameterization employed in CRHM previously by Pradhananga and Pomeroy, (2022b, 2022a)
318 in that sub-daily fluxes can have important contributions to seasonal melt. If the snowpack is not
319 completely melted by the end of the summer, the snow becomes firn. Firn densification occurs through a
320 5-layer system, with density increasing from 450 to 850 kg m^{-3} . The densification rate was set to 100 kg
321 $\text{m}^{-3} \text{yr}^{-1}$ to be consistent with observations.

322
323 Further addition to the CRHM model of PGRB is the inclusion of melt under debris-cover, calculated
324 following the empirical equation of Carenzo *et al.* (2016). This formulation was shown to have similar
325 results to an energy-balance approach treating the energy transfer as conductive energy flux, driven by
326 the conductivity of the debris layer and the temperature gradient (Reid and Brock, 2010). Ice-cored
327 moraines are another type of debris-covered ice, a common feature in mountain environments (Østrem
328 *et al.*, 1970; Gruber and Haeberli, 2009). In the PGRB, Hopkinson *et al.* (2012) found that runoff from the
329 periglacial areas accounted for 8% of the water losses from basin storage for the period 2000 to 2010.
330 Debris cover thickness in the PGRB was obtained from multiple point measurements over the study area
331 from ice cliffs and manually digging pits during field site visits. The debris thickness varied from thin debris
332 (5-10 cm thickness) in steep areas and on the edge of the medial moraine, to value of 0.5 meter in the
333 main area of the medial moraine. In the debris-covered area on the western side of the glacier toe, the
334 maximum debris thickness measured was of 1.4 m, with an average of 0.53 m (Aubry-Wake *et al.*, 2022).

335
336 For each glacier HRU, runoff water (rainfall on glacier area and meltwater) is routed vertically through the
337 snow, firn and ice reservoir to the glacier-rock interface using a linear reservoir approach (Hock and
338 Noetzli, 1997). Each layer (snow, firn and ice), and for each HRU, has its own reservoir with a static value
339 for the duration of the simulation. The snow reservoir of each HRU is connected laterally to other HRUs
340 through blowing snow and avalanching mass fluxes, but the ice and firn reservoirs are not connected
341 laterally to other HRUs as there is no ice dynamics implemented in this model. Due to the fast routing
342 observed in this basin, these storage values are set to zero. Once the ice thickness of a glacier HRU reaches
343 zero, the cover type is automatically converted to bare rock without interrupting the simulation. The
344 elevation of the glacier HRUs evolves following the surface melt or accumulation throughout the
345 simulation. For the glaciers HRUs that melt out during the simulation, the initial ice volume was
346 determined to match the year of glacier retreat based on the glacier outlines for 2005 and 2017 (Fig. 1a).
347 For example, the ice thickness in HRU 9, corresponding to the glacier toe, was set to completely melted
348 out by 2005.

349
350 **2.2.2.4. Infiltration and subsurface flow and storage**
351 Once the snow and ice meltwater and rainfall runoff reach the glacier-rock interface of individual HRUs,
352 the water is routed through the soil module to produce surface runoff, infiltration and subsurface runoff
353 as per Fang *et al.* (2013). Similarly, the snowmelt and rainfall runoff from the non-glacierized HRUs,
354 composed of rock debris and exposed bedrock, is also handled by the soil module. Infiltration into
355 unfrozen soils is calculated following Ayers (1959) and into frozen soils following Gray *et al.* (2001). For
356 unfrozen soil (Ayers, 1959), alpine soil texture parameters were transferred from Marmot Creek Research
357 Basin, further south in the Canadian Rockies (Fang *et al.*, 2013). Frozen and thawed soil moisture initial
358 conditions for storage and moisture content were obtained using a one-year spin-up period (1987).

359
360 The soil module is divided into a recharge layer, from which evapotranspiration can occur, a subsurface
361 and a groundwater layer. Each soil layer, for each HRU, has a storage volume and a saturated hydraulic
362 conductivity which dictate the fate of the meltwater and rainfall-runoff for each HRUs: saturation excess
363 water becomes surface runoff routed to another HRU, whilst infiltrated water contributes to subsurface

364 runoff and groundwater flow. Groundwater recharge occurs via percolation from the soil layers and
365 groundwater discharge takes place through horizontal drainage in the groundwater layer. Subsurface
366 discharge occurs via horizontal drainage from either soil layer, with the lateral flow calculated using
367 Darcy's law for unsaturated flow, as described by Fang *et al.* (2013). Surface runoff forms when melt or
368 rainfall rates exceed the infiltration rate (infiltration excess surface runoff) or when they exceed the
369 subsurface withdrawals from saturated soils (saturation excess surface runoff). The presence of water
370 ponding in surface depressions has been observed in the moraine, the ice-cored moraine and the low
371 angle talus environments. This was represented in the model as a depressional storage capacity set for
372 these HRUs. When depressional storage capacity is present, surface runoff refills this storage before it
373 can contribute to downstream runoff.

374
375 The soil module was parametrized based on the cover types in the basin: clean ice, debris-covered ice,
376 steep talus, low angle talus, moraine and cliffs (Table 1). For the clean ice HRUs, the glacier was assumed
377 to be sitting on bedrock with minimal subglacial debris, and therefore, was given low storage volume. For
378 the debris-covered glacier HRUs, the subsurface layer storage was set to a volume varying with debris
379 thickness to represent moisture storage in the debris layer, as the debris-layer does not have a reservoir
380 layer of its own. For the talus and moraine non-glacierized HRUs, the recharge soil layer was set to
381 represent the coarse and shallow surface rock debris, and the subsurface layer was set to represent the
382 thicker underlying moraine and talus debris, following field observations. The storage parameters for talus
383 and moraine land cover were based on extensive studies of talus and moraine groundwater flow
384 processes at Lake O'Hara Research Basin in the Canadian Rockies (McClymont *et al.*, 2010; Langston *et al.*,
385 2011; Muir *et al.*, 2011; Hood and Hayashi, 2015). Moraine deposit HRUs were set to have the largest
386 storage capacity, being composed of coarse to fine sediment size. The storage in steep talus slopes
387 (coarse, irregular rocks with large void space) HRUs was set to small values based on Langston *et al.* (2011),
388 who found talus slopes to have a thin saturated layer (0.01 - 0.1m) at the bedrock-talus interface, which
389 quickly transmits water to the downslope environment. This low storage capacity increases for low-angle
390 talus HRUs, where micro-topographies can enhance water storage. Minimal soil storage was assumed for
391 the cliff HRUs, as these are bedrock with limited debris moisture storage. The storage of groundwater
392 layer, set to represent the bedrock storage, was set to the same value across the basin and reflects the
393 porous limestone lithology of basins in the region (Fang *et al.*, 2013).

394
395 The saturated hydraulic conductivities for talus and moraine sediments were transferred also from Lake
396 O'Hara (McClymont *et al.*, 2010; Langston *et al.*, 2011; Muir *et al.*, 2011). Talus fields studied in the
397 Canadian Rockies had a very high hydraulic conductivity (0.01-0.03 m s⁻¹) (McClymont *et al.*, 2010), with
398 similar values obtained by Clow *et al.* (2003) in a talus and rock-glacier dominated basin in the Colorado
399 Rockies.

400 [Table 1 near here]

401
402 **2.2.2.5. Routing**
403 Routing of runoff from the surface and subsurface layers between the HRUs is handled in CRHM by
404 Clark's lag and route algorithm (Clark, 1945, Pomeroy *et al.*, 2007) following a user-specified routing
405 order. This user-defined order means that water in the soil, subsurface and groundwater layer can move

406 laterally between HRUs to simulate the flow of water through the basin, from higher elevation to lower
407 elevation and converging towards to basin outlet. In this implementation of CRHM, no stream channel
408 exists, and the basin outflow was calculated as the water leaving the outlet HRU (HRU 10, Fig 1b). For
409 each HRU, water that infiltrated into the groundwater reservoir was assumed to leave the basin as
410 groundwater flow in a “leaky basin” and was not captured at the basin outlet streamflow, or the
411 simulated streamflow compared to measured streamflow.

412 The lag and route method translates each HRU’s inflow into outflow based on a lag time and a storage
413 constant. Considering the flashiness of the system, with meltwater reaching the outlet of the basin in a
414 few hours to half a day (Ommanney, 2002; Munro, 2011, 2013), the routing through the basin was
415 assumed to occur within a day, the minimum timestep at which the streamflow was analyzed. To
416 capture this fast routing, the routing parameters (lag time and storage constant) for snow and ice melt
417 as well as surface and subsurface flow were set to zero. The groundwater reservoir storage constant
418 was set to 10 days for low-angle HRUs and 5 days for steep HRUs based on the physical understanding of
419 alpine groundwater flow and storage (Hayashi, 2020).

420 **2.3. Assessing model performance**

421 Using multiple lines of evidence to evaluate model performance is critically important to reduce internal
422 inconsistencies and improve model fidelity (Finger et al., 2011; Schaepli and Huss, 2011; Pellicciotti et al.,
423 2012; van Tiel et al., 2020b). The model was evaluated using four sets of observations relating to snow
424 accumulation and ablation, glacier melt, and streamflow. Snow accumulation and glacier melt across the
425 glacier area were assessed using point mass balance measurements by the Geological Survey of Canada
426 for the period 2005-2018 (Figure 2a-b). 240-point measurements for winter and 163 for summer mass
427 balance were made using drilled, surveyed stakes between elevation 2136 and 2760 m.a.s.l. For the years
428 1989-1995, the mean mass balance by elevation band was used to evaluate model performance. The
429 simulated summer and winter mass balance were extracted for the same date as the recorded
430 measurements, generally corresponding to late April or early May for winter mass balance and late
431 September for summer mass balance surveys.

432
433 Model evaluation is done with a range of metrics as appropriate for each dataset. The Nash Sutcliffe
434 efficiency (NSE, Nash and Sutcliffe, 1970) is calculated as follow:

$$436 \quad NSE = 1 - \frac{\sum_{t=1}^{t=T} (x_{sim}(t) - x_{obs}(t))^2}{\sum_{t=1}^{t=T} (x_{obs}(t) - \bar{x}_{obs})^2} \quad (\text{Eq. 2})$$

437
438 where T is the total number of time steps, $x_{sim}(t)$ the simulated streamflow at time t , $x_{obs}(t)$ the observed
439 streamflow at time t , and \bar{x}_{obs} the mean observed discharge. A value of $NSE = 1$ indicates perfect
440 agreement between simulations and observations while $NSE = 0$ indicates that the model simulations have
441 the same explanatory power as the mean of the observations, and $NSE < 0$ indicates that the model is a
442 worse predictor than the mean of the observations (e.g., Schaepli and Gupta, 2007).

443
444 The Kling-Gupta Efficiency (KGE, Gupta *et al.*, 2009) is also used to evaluate model performance:
445

$$KGE = 1 - \sqrt{(r - 1)^2 + (\alpha - 1)^2 + (\beta - 1)^2} \quad (\text{Eq. 3})$$

where r is the linear correlation between observations and simulations, α is a measure of the flow variability error, and β relates to the bias. KGE can also be written as:

$$KGE = 1 - \sqrt{(r - 1)^2 + \left(\frac{\sigma_{sim}}{\sigma_{obs}} - 1\right)^2 + \left(\frac{\mu_{sim}}{\mu_{obs}} - 1\right)^2} \quad (\text{Eq. 4})$$

where σ_{obs} is the standard deviation in observations, σ_{sim} the standard deviation in simulations, μ_{sim} is the simulation mean, and μ_{obs} is the observation mean. $KGE > -0.41$ indicates that the simulated variable is performing better than the average of the observations and therefore, the model has predictive power, and a $KGE < -0.41$ indicates a poor model performance (Knoben *et al.*, 2019). Additionally, the root mean square error (RMSE), the Spearman's rank correlation coefficient (r) and the mean bias (MB) are calculated.

2.4. Assessing trends and variability in hydrometeorological conditions

The presence of significant trends in annual or seasonal air temperature, precipitation and streamflow was assessed using the non-parametric Mann-Kendall significance test at a significance level of $\alpha = 0.05$. The magnitude of the detected trends was estimated using Sen's slope (Sen, 1968), which calculates the slope using the median of all pairwise slopes in the data set. The seasons for the trend analysis were defined as fall (SON), winter (DJF), spring (MAM) and summer (JJA).

To gain further information on the variability in the streamflow generation processes in the basin, meteorological conditions and melt patterns in years of high streamflow (HF) were compared to those of low streamflow (LF). Years with volumes greater than the mean plus one standard deviation were considered to be high flow (1992, 1994, 2006, 2013, 2015, 2016) and years with volumes less than the mean minus one standard were considered to be low flow (1995, 1996, 1997, 2000, 2003, 2008).

3. RESULTS

3.1. Model evaluation

For both the mass balance points available as the mean balance by elevation bands (measured gradient, year 1989-1995 in Fig 2), and for the mass balance points measured at individual stakes (measured point, years 2003-2017 in Fig2), linear regressions were used to calculate the annual measured mass balance elevation gradient, defined as the rate of change in mass balance with elevation (Fig 2). A variability envelope was calculated as ± 2 standard deviations around the residuals from the calculated linear regression values (Fig 2a). These variability envelopes were used to assess if the fluctuations from the background elevation gradients were similar between the measured and modelled point mass balance.. 77% of the modelled winter mass balances fall within this envelope. In most years, the modelled winter mass balance agrees with the measurements, but for some years, such as 1989, 1994 and 2009, there is

486 minimal overlap between measured and modelled winter mass balance. The calculated and modelled
487 winter mass balance gradients were compared for the 19 available years between 1995 and 2017. The
488 average gradients are similar, with the calculated gradient of 0.14 m.w.e. per 100 m elevation being similar
489 to the modelled gradient of 0.13 m.w.e., with an RMSE of 0.04 m.w.e. per 100 m elevation gain and a
490 correlation coefficient of 0.21. The model has a slight tendency to underestimate the measured gradient
491 with a mean bias of -0.07 m.w.e. The largest difference between modelled and measured winter mass
492 balance occurred at ~2600 m.a.s.l. and was likely due to the influence of avalanching. Mass balance
493 observations deliberately avoid avalanche-prone areas and so do not reflect this source of variability, even
494 though avalanche deposits have been noted at this elevation in field observations and historical reports
495 (Young, 1977). Therefore, the winter mass balance simulated by CRHM, which account for snow
496 redistribution by gravity, will be more variable than the measured mass balance points at the same
497 elevation. Additionally, evaluation of snow accumulation at the highest elevation HRU is restricted by the
498 lack of measurements above the altitude of 2760 m. Considering that point winter mass balance
499 measurements can vary by up to 0.2 m w.e. over distances of a meter at Peyto Glacier (Young, 1977; Demuth
500 and Keller, 2006), the modelled winter balance is considered to have been simulated in a satisfactory
501 manner. .

502

503 For summer mass balance, 92% of the modelled values for the 2007-2013 period, or 97 of the 108 values,
504 fit within the variability envelope of the measured stake balances (Fig 2b). Despite most of the modelled
505 values fitting within the range of measured values, the mass balance gradient for summer mass balance
506 was consistently larger than the measured one, with a mean modelled gradient of 0.88 m.w.e. per 100 m
507 elevation gain being larger than the mean modelled rate of 0.54 m.w.e., with an RMSE of 0.39 m.w.e.,
508 mean bias of 0.63 m.w.e. and a correlation coefficient of -0.04. The gradient standard deviation is larger
509 for the measurements (0.58 m.w.e.) than for the modelled values (0.38 m.w.e.).

510

511 *[Figure 2 near here]*

512

513 *[Figure 3 near here]*

514

515 A comparison of modelled snow depth with snow depth measured at the on-ice AWS for the 2011-2020
516 winters yielded a Nash-Sutcliffe efficiency (NSE) ranging between 0.49 and 0.84 and a coefficient of
517 determination (R^2) between 0.62 and 0.98 (Fig.3a). For the nine periods with surface melt measurements
518 from the on-ice AWS, which cover a total of 981 days, the correlation coefficient of observations with
519 modelled ice melt at glacier toe is 0.99, with a mean bias of 0.09 m.w.e., a root mean square error (RMSE)
520 of 0.43 m.w.e. and an NSE of 0.90 (Fig. 3b-f). Overall, the set of evaluations of modelled snow
521 accumulation and snow and ice ablation shows that the model can appropriately represent snow and ice
522 dynamics on the glacier.

523

524 Modelled streamflow at the basin outlet was compared to the measured streamflow for the 2013-2020
525 melt seasons (Fig 4). Streamflow measurement was only available during the snow-free season and did
526 not allow a model evaluation for the earliest and latest seasonal low flow or melt events. For the eight

527 melt seasons, the simulations compared to observations with a NSE of 0.69, with annual results ranging
528 from 0.41 to 0.87. RMSE for the entire period was $0.98 \text{ m}^3 \text{ s}^{-1}$, ranging between 0.66 and $1.2 \text{ m}^3 \text{ s}^{-1}$ and
529 the mean bias ranged from -0.24 to 0.35. The Kling-Gupta efficiency (KGE, Gupta *et al.*, 2009) ranged
530 between 0.09 to 0.45 for individual years and averaged 0.15 for the entire period. When considering the
531 three components of the KGE, the largest values, indicating stronger performance, are found for the bias
532 (β) and relativity term (α), with lower values corresponding to the correlation term r . Considering that
533 high NSE values are expected for a basin with a strong seasonal cycle, as demonstrated by Schaefli *et al.*
534 (2005), and further discussed in Schaefli and Gupta (2007) and Seibert *et al.* (2018), the NSE performance
535 of the CRHM model was compared with that of a simple benchmark model calculated as the mean
536 observed discharge for each calendar day (DOY average benchmark model, as discussed in Garrick *et al.*,
537 1978; WMO, 1986; Schaefli and Gupta, 2007). In other words, two NSE values were calculated: a regular
538 NSE with the simulated streamflow, and a benchmark NSE using the DOY average streamflow values. If
539 the benchmark NSE is higher than the regular NSE, then the simulated streamflow shows a lower
540 predictive capacity than the average DOY values. In this case, the DOY average benchmark model
541 performed more poorly than the CRHM model for 7 out of the 8 years available, with its average NSE
542 lower than that of the CRHM model by 0.14, providing further evidence that CRHM can capture both the
543 seasonality of the flow regime and the smaller-time scale fluctuations. Modelled groundwater flow is also
544 shown.

545

546

547

548 *[Figure 4 near here]*

549

550 **3.2. Basin hydrometeorological variability**

551 **3.2.1. Annual conditions and trends**

552 The basin has a cold climate, with annual mean air temperature staying below 0°C for the whole study
553 period, ranging between -5.0 and -2.3°C (Fig 5a). Only the lowest elevations in the basin, below 2200
554 m.a.s.l., have an annual mean air temperature above zero, varying from -1.67 to 1.00°C . Summer
555 temperature in the basin can reach up to 23.4°C . The precipitation regime in the basin is dominated by
556 snowfall, which contributes an average of 85% to the total precipitation (Fig 5b). This ratio increases to
557 89% snowfall in the highest elevation of the basin (above 2700 m.a.s.l.) and decreases to 68% in the lowest
558 elevations (below 2200 m.a.s.l.).

559 *[Figure 5 near here]*

560

561 As shown in Figure 5c, annual area-weighted streamflow expressed as water equivalent depth over the
562 PGRB, also known as water yield, varied from 3240 mm yr^{-1} , in 1988, to 1870 mm yr^{-1} , in 1996. On average,
563 snowmelt, both on and off the glacier, contributed the largest volume and fractional contribution, 44-
564 89%, to annual streamflow. Ice melt from the glacier and ice-cored moraine contributed 10-45%. Firn melt
565 and rainfall-runoff each contributed 13% or less to annual streamflow, with firn melt ranging from 0-13%
566 and rainfall-runoff and infiltration contributing 1-12% of annual streamflow. Rainfall-runoff represents
567 only rainfall on snow-free surfaces (glacier or bare-ground) as rain-on-snow contributes to the snowpack

568 dynamics including refreezing, melting and discharge from the pack depending on the thermodynamic
569 state and porosity of the snowpack. The modelled streamflow components were calculated before the
570 routing routine was applied and therefore, do not reflect streamflow mixing, but runoff sources in the
571 basin. The snow, firn and ice melt originating from the glacier area, grouped as “glacier runoff”, provide a
572 disproportionate amount of streamflow, as the glacier covers only 56% of the basin area but the glacier
573 runoff provides on average 71% of annual streamflow. Only two out of the 33 years analyzed showed a
574 positive mass balance. For the remaining years glacier wastage varied from 6 to 77% of basin yield, with
575 an average of 53%. Glacier wastage was calculated following Comeau *et al.* (2009) and defined as the
576 volume of ice and firn melt exceeding the annual volume of snow accumulation on the glacier and causing
577 an annual net loss of glacier volume. Basin yield was calculated as the combined streamflow at the basin
578 outlet and groundwater discharge leaving the basin. Surface streamflow at the outlet contributed on
579 average 63% of basin yield, while groundwater discharge contributed 37%. The detailed calculate of
580 wastage and shown in Appendix B.

581
582 Figure 6 showed significant hydrometeorological trends ($p < 0.05$); at the basin scale, summer
583 temperature increased from 3.50 °C to 4.55 °C over 1988-2020. Over the same time period, winter
584 snowfall decreased by 286 mm, and summer and annual rainfall increased by 179.6 and 152.1 mm
585 respectively. Despite the trends in precipitation phase favouring rainfall, no trends were found in annual
586 air temperature or annual precipitation depth over 1988-2020.

587
588 [Figure 6 near here]

589 **3.2.3. Seasonal meteorological conditions and streamflow correlation**

591 Further analysis examined the associations between annual streamflow volume and annual and seasonal
592 meteorological variables (temperature, rainfall, snowfall). Annual, spring and summer temperature,
593 summer rainfall and winter snowfall were the only forcing meteorological variables significantly
594 correlated to annual streamflow (Table 2, Fig. 7). Winter snowfall was negatively correlated with
595 streamflow, the opposite of what would be expected for a snowmelt-dominated non-glacierized basin.
596 Ice melt, firn melt and rainfall-runoff were the only runoff components significantly correlated to annual
597 streamflow (Table 3, Fig. 7). In addition, the timing of the glacier exposure was strongly negatively
598 correlated with streamflow. The timing of ice exposure was quantified as by the day of year (DOY) by
599 which the winter snowpack has fully melted in the mid- and upper glacier area of the basin, with HRU 3
600 selected as representative. Ice melt and timing of ice exposure were most strongly correlated to the
601 annual streamflow, followed by the rainfall-runoff and firn melt. Even though snowmelt provides the
602 greatest fraction of annual streamflow, no significant correlation was found between snowmelt and
603 streamflow.

604
605 In 5 of the 33 years analyzed, the snow outside of the glacier area did not completely melt throughout the
606 summer and carried over to the following year. On the glacier, this leftover snow turned to firn, and
607 influenced surface melt in the following summer by having a different albedo and density than either
608 snow or ice. However, the influence of this leftover snow on the following year’s streamflow appeared to

609 be minimal in the PGRB as no significant correlation was found between the snow remaining in the basin
610 just before the transition to firn and the following years' streamflow (Table 3).

611

612 *[Figure 7 near here]*

613

614 *[Table 2 near here]*

615

616 *[Table 3 near here]*

617

618 **3.4 Contrasting high and low streamflow years**

619 High flow years were on average 1.43 °C warmer than the years with low flow, with the largest difference
620 in January, March and April (Fig 8a). The HF years received 143 mm more rainfall and 295 mm less snowfall
621 than the LF years, (Fig 8b-c). The differences in precipitation and temperature are reflected in snowpack
622 ablation (Fig 7d). Starting in December, HF and LF snowpack regimes diverge. The HF snowpacks reached
623 a peak SWE of 957 mm in mid-April, whilst the LF snowpacks continued to accumulate until early May
624 when they reached a peak SWE of 1330 mm. Both HF and LF snowpacks follow similar ablation patterns
625 over the melt season and by September 1st, the remaining snowpack starts to transform into firn. In LF
626 years, the remaining snowpack was 213 mm SWE at this transition date, whilst in HF years no snow
627 remained. Using the non-parametric Wilcoxon signed rank test (Gibbons and Chakraborti, 2010), the
628 differences in monthly air temperature, snowfall and SWE (but not monthly rainfall) between HF and LF
629 years were significant at the alpha = 0.05 level.

630

631 *[Figure 8 near here]*

632

633 Differences in the sources of streamflow were also analyzed between LF and HF years (Fig 9). Annual
634 streamflow volumes were 41% greater in HF years than LF years. Snowmelt provided by far the greatest
635 source of streamflow, but its contribution differed by only 1% between LF and HF years and so did not
636 substantially contribute to interannual variability in streamflow volumes. Differences in snow ablation
637 regime between HF and LF years were apparent; snow ablation started 10 days earlier in HF than in LF
638 years, with rapid melt and depletion of snow occurring 15 days earlier, in mid to late summer. The earlier
639 snow ablation in HF years exposed glacier ice earlier and led to a greater ice exposure by late summer,
640 increasing basin-averaged, late summer ice melt rates from 9 mm d⁻¹ in LF to 17 mm d⁻¹ in HF years (Fig
641 9b). As a result, the volume of ice melt was 103% greater in HF than in LF years. Similarly, the firn melt
642 contribution to streamflow was 162% greater in HF compared to LF years, with nearly double the peak
643 melt rate (2.3 compared to 1.4 mm d⁻¹) and an almost one-month earlier start to firn melt. Consistent with
644 greater rainfall, rainfall-runoff was 145% higher in HF years. Even though firn melt and rainfall-runoff
645 were greater in HF years by a larger fraction than other streamflow sources, their enhancement of
646 streamflow was modest as together they contributed less than 10% of streamflow volume. In contrast,
647 ice melt had smaller fractional increases for HF years, but a much stronger impact on differences in
648 streamflow volumes and timing.

649

650 LF years were colder, with higher snowfall and lower rainfall. The deeper LF year snowpack combined with
651 a delayed onset to melt due to colder spring temperatures resulted in snowpacks persisting later in the
652 summer in LF than in HF years. This caused less glacier ice to be exposed and ice exposure to occur later
653 in the melt season, such that its melt contributed less to streamflow. Additionally, LF years received lower
654 rainfall. Initial meteorological forcings, differing snow accumulation and depletion patterns, and resulting
655 rates and durations of rainfall-runoff, snowmelt, ice melt and firn melt interacted to cause large
656 streamflow volumetric differences between HF and LF years.

657
658 *[Figure 9 near here]*

659 **3.5. Assessing uncertainty of the subsurface storage parameterization**

661 The parameters with the higher uncertainty in the application of the PGRB are the ones associated with
662 non-existent or sparse observations in the basin, preventing the evaluation of these individual processes.
663 This is particularly the case for the surface water-groundwater interactions and the subsurface routing.
664 The surface water-groundwater interactions were parametrized to represent a physical understanding of
665 alpine groundwater systems based on field knowledge from the PGRB and in-depth studies from similar
666 landscapes in the Canadian Rockies, but the lack of direct observations of soil moisture and groundwater
667 storage within PGRB precludes an in-depth evaluation of this model component. Therefore, the
668 uncertainty associated with these parameters was tested. The storage capacity and routing delays of the
669 different land covers, shown in Table 2, were varied and the resulting change in simulated streamflow
670 was assessed in a scenario-based parameter uncertainty assessment (Table 4). Doubling the soil storage
671 decreased streamflow volume by less than 5% and decreasing soil storage by half increased streamflow
672 by 8.8%. However, either doubling or reducing by half the soil storage volume also influenced the
673 groundwater discharge from the basin, changing both the timing and the total volume of groundwater
674 flow by up to 17% compared to the main simulation. When the soil storage increased whilst the
675 groundwater storage decreased, or the converse, the change in groundwater flow timing and volume was
676 limited to below 4%. However, when the total basin subsurface storage either increased or decreased,
677 groundwater flow changed by up to 30% compared with the baseline simulation. Given the sensitivity of
678 basin groundwater to the subsurface storage parametrization and sparse high elevation groundwater
679 observations, further investigations should assess the transferability of storage parameters for
680 groundwater routing in high alpine basins.

681
682 *[Table 4 near here]*

683 **4. Discussion**

684 **4.1. Measurements, process representation and parameter uncertainty**

685 The comprehensive processes in the physically based modelling approach used here were included to
686 reduce model uncertainty; these processes were represented with substantial spatial discretization, and
687 process identification and parametrization were based on extensive fieldwork. In the attempt to
688 comprehensively represent the physical system in the PGRB, it is expected that uncertainty was reduced
689 by selecting appropriate methods and models instead of through more traditional, and sometimes
690

691 complex, calibration procedures (Kirchner, 2006; Clark *et al.*, 2016). Despite this, model prediction errors
692 can still accrue through inaccuracies in measurements, process representations and parameters (Beven,
693 2016). The main elements in the modelling procedure relating to these sources of uncertainty are
694 discussed below.

695

696 **4.1.1. Limitations of the observational data**

697 A large amount of input data is needed to parametrize and evaluate model simulations but obtaining high-
698 quality observational data from remote glacierized mountain basins is an extraordinary challenge. In the
699 PGRB, the long-term meteorological measurements from the network of on-ice stations are invaluable to
700 investigate the temperature patterns across the basin, but the lack of distributed precipitation
701 observations increases uncertainty. Because of this lack of information on the spatial distribution of
702 precipitation, the end-of-winter SWE elevation gradient is used as a proxy for the precipitation elevation
703 gradient. As the SWE elevation gradient considers snow redistribution by wind and gravity, mid-winter
704 melt and sublimation, this approach causes a source of error in the precipitation gradient. Further
705 uncertainty is caused by the use of reanalysis data for precipitation instead of in-situ data. Gridded
706 precipitation datasets are known to be highly uncertain in mountain regions, particularly at high
707 elevations (Lundquist *et al.*, 2015; Henn *et al.*, 2018). Even though the ERA-Interim precipitation was bias-
708 corrected to in-situ observations, ensuring reasonable monthly cumulative volume, the short rainfall
709 events occurring in spring, summer and fall months might have not been adequately captured by the
710 gridded precipitation, resulting in further uncertainty in the model forcing data. Additional measurement
711 of seasonally variable precipitation gradient in the PGRB would be a valuable information to improve
712 model parametrization.

713

714 Streamflow information was also limited by the persistence of snowdrifts in the channel, preventing the
715 evaluation of model performance for the early-season and late-season streamflow processes. The
716 uncertainty linked with measuring streamflow in a dynamic, proglacial landscape also increases the
717 uncertainty in developing a robust rating curve, which was mitigated by obtaining several salt-dilution
718 measurements over three melt seasons and a careful assessment of the measurement quality. The
719 simulated glacier winter and summer mass-balances at the higher elevation in the basin are also not well
720 constrained, as there is a lack of measurements at these altitudes due to the difficult access through
721 avalanche and crevassed terrain.

722

723 **4.1.2. Limitations in the CRHM process representation and parametrization**

724 The precipitation gradient used is fixed in the model, but there is evidence that mountain precipitation
725 gradients vary seasonally and annually based on the processes controlling the precipitation events (Houze,
726 2012; Pepin *et al.*, 2022). The lack of temporally variable precipitation gradient could explain the variable
727 performance of the simulated end-of-winter snow elevation gradient, with some years failing to capture
728 the measured snow accumulation gradient. However, the lack of information on the variability of the
729 precipitation gradient prevented varying this gradient in the modelling framework. The measured mass
730 balance gradient was also more variable than the modelled one, which suggests that elevation has a
731 greater role in controlling melt in the model than is observed. This could be due to deviations from reality

732 in model parameters such as albedo or gradient settings for precipitation and/or temperature and/or
733 other errors.

734
735 The meltwater routing through the glacier as applied in this model, a static linear reservoir storage for the
736 snow, firn and ice layer, is a simplification of the complex subglacial and englacial drainage system. Despite
737 its simplicity, the routing approach used here captures the fast drainage of the system at the daily
738 timescale. However, the current configuration of the CRHM glacier melt and routing preclude an analysis
739 of the sub-daily streamflow variation. One option to improve the physical realism of the glacial meltwater
740 routing could be to include a transient storage parametrization based on SWE or time of year to reflect
741 the developing englacial and subglacial drainage system of the glacier, as in Stahl *et al.* (2008). A
742 combination of dye and hydrochemistry tracing experiments could provide insights in the flow path of
743 meltwater through the glacier system (Fyffe *et al.*, 2019a, b; Nienow *et al.*, 1993).

744
745 Another model improvement that would improve the glacier module process representation would be to
746 implement ice-flow dynamics in the simulations. In this case, the glacier area was constrained by satellite
747 imagery, and the predominantly negative mass balance even at the higher elevation in the basin avoided
748 the infinite accumulation of snow in the accumulation area, a problem that can occur when ice-flow
749 dynamics is not implemented. Further work should be conducted to implement and test an ice flow
750 routine.

751
752 The lack of soil moisture and groundwater observations in the basin limit the evaluation of surface water-
753 groundwater interaction and prevents a thorough assessment of the possibility of a “leaky catchment”
754 (Fan, 2019). Groundwater contributions and surface water-groundwater interactions could contribute to
755 the bias in simulated streamflow volumes. The fate of groundwater in alpine basins in the Canadian
756 Rockies has been suggested to be mostly limited to local, shallow aquifers in coarse deposits connecting
757 first- and second-order streams (Hayashi, 2020), but some studies have suggested that glacier basin
758 groundwater recharges regional and mountain block aquifers (Castellazzi *et al.*, 2019; Campbell and Ryan,
759 2021). Considering both possibilities, the water entering the groundwater system in the PGRB simulations
760 could contribute to unmeasured streamflow just downstream of the basin outlet and contribute to the
761 Peyto Lake water budget or form regional flow networks resurfacing further downstream.

762
763 **4.2. PGRB trends and compensatory behaviour**

764 The absence of temporal trends in annual air temperature and precipitation in this study contrast with
765 most findings in the Canadian Rockies (Harder *et al.*, 2015). DeBeer *et al.* (2016) found a 2 °C increase in
766 air temperature and a 14% precipitation increase in this region for the period 1950-2015. Pradhananga
767 and Pomeroy (2022a) contrasted the hydrology of the PGRB between the 1960s and the 2010s and found
768 an increase of 260 mm (16%) in streamflow with a 226 mm (16%) decrease in precipitation. The difference
769 in trends is most likely due to the different periods analyzed and the methodologies used. However, for
770 35 basins in the Columbia River headwaters, located southwest of the PGRB in the adjacent Selkirk and
771 Monashee mountains, Moore *et al.* (2020) did not find significant trends at $p < 0.05$ in August air
772 temperature for the 1977-2017 period, but found a significant decreasing trend at $p < 0.05$ in August

773 precipitation, which is similar to the trends found for summer rainfall and summer temperature in this
774 study. For streamflow components, significant increasing trends were found for summer rainfall-runoff,
775 summer ice melt, and winter snowmelt, and a decreasing trend was found for summer snowmelt, but no
776 trends were found for seasonal or annual streamflow. This is consistent with Naz *et al.* (2014), who did
777 not find significant trends in streamflow for the years 1981-2007 for the upper Bow River at Lake Louise,
778 a 422 km² basin adjacent to the PGRB. These results contrast with findings by Moore *et al.* (2020) and
779 Stahl and Moore (2006), who found decreasing trends in August streamflow for glacierized basins in
780 mountain ranges west of the Continental Divide. The difference in these trends might be linked to the
781 different snow accumulation and weather patterns occurring on either side of the Continental Divide;
782 conditions are typically colder and drier on the eastern slopes, but also to the difference in time period
783 analyzed (only August versus summer period)

784
785 Even if some trends were observed in the summer air temperature, winter snowfall, summer rainfall, and
786 in certain streamflow components in the PGRB, no trend was noticeable in the net annual streamflow
787 volumes. This suggests that, for the period studied, there might be compensating effects amongst the
788 hydrological processes and such that the net flow components generating basin streamflow have been
789 relatively insensitive to environmental change. Harder *et al.* (2015) found evidence for such cold regions
790 compensatory behaviour in the unglacierized Marmot Creek Research Basin in the Canadian Rockies
791 which dampened its streamflow response to changing climate and land cover. Natural climate variability
792 might also have concealed the streamflow trend, as discussed by Fatichi *et al.* (2014), who found that
793 natural climate variability obscured climate-driven changes in streamflow by up $\pm 20\%$ in the Alps.

794

795 **4.3. Linking PGRB flow variability with hydrological processes**

796 Within the PGRB, the lack of correlation between snowmelt and streamflow, combined with the highly
797 significant correlation of streamflow to summer meteorology, suggests that summer hydrometeorological
798 and glaciological conditions play an important role in governing the inter-annual variability of streamflow.
799 This is consistent with results from Europe by Farinotti *et al.* (2012) who analyzed nine alpine glacierized
800 basins in the Alps and found that annual streamflow and precipitation were not significantly correlated
801 for basins with glacierized areas over 40%, but that summer air temperature and annual streamflow were
802 well correlated for basins with a glacierized area above 35%. In the highly glacierized Nordic Creek basin,
803 located 85 km west of the PGRB in the Selkirk Mountains of British Columbia, glacier wastage
804 contributions to streamflow were also found to be highly variable year-to-year (Moore *et al.*, 2020).

805
806 The influence of winter conditions on streamflow variability was also noticeable through the significant
807 negative correlation of streamflow with winter snowfall and timing of ice exposure rather than snowmelt
808 or peak snow water equivalent. It should be noted that not all snowfall will form snowmelt in high snowfall
809 years and so snowfall is more variable than snowmelt. The negative correlation between winter snowfall
810 and streamflow volume is due to the control that snowfall exerts on the timing of summer ice exposure,
811 as confirmed by the strong negative correlation between timing of ice exposure and streamflow. In low
812 snowfall years, glacier ice is exposed earlier, and due to its lower albedo, the surface melt is enhanced,
813 leading to higher annual streamflow. This correlation is possible when the additional melt from exposed

814 glacier ice in low snowfall years exceeds the reduction in snowmelt from the glacier and non-glacier
815 fractions of the basin.

816
817 The variability between low flow years and high flow years was a combination of hydrological processes.
818 In addition to LF years receiving lower rainfall, initial meteorological forcings, differing snow accumulation
819 and depletion patterns, and resulting rates and durations of rainfall-runoff, snowmelt, ice melt and firn
820 melt interacted to cause large streamflow volumetric differences between HF and LF years. This result is
821 consistent with the findings of Pradhananga and Pomeroy (2022) who found that with warming conditions
822 from the 1960s to current times, glacierized basin streamflow in the Canadian Rockies was increasing
823 despite declining precipitation and snowmelt, the difference being sustained by greater ice melt.

824 825 **4.4. Comparing flow composition**

826 The flow composition fractions calculated in this study, with snowmelt contributing 44-89% to annual
827 streamflow, ice melt contributing 10-45% and firn melt and rainfall-runoff contributing to 13% or less, are
828 consistent with other studies, even though a comparison of streamflow composition between studies is
829 complicated by the range of methods that can be used to define the streamflow components (Frenierre
830 *et al.*, 2013), by the varying definitions of “glacier runoff” (Radic and Hock, 2014), and the varying temporal
831 and spatial scale investigated. A previous study by Comeau *et al.* (2009), conducted on macro-scale basins
832 located in the Canadian Rockies, showed that July-September glacier runoff (snow and ice melt from the
833 glacier area) contributed 73-83% of the streamflow in basins with more than 10% glacier cover. For the
834 Peyto Creek basin, corresponding to a slightly larger basin than the one investigated in this study, they
835 additionally found that for the 1973-1977 period, glacier wastage flux (or the net glacier water storage
836 lost from negative mass balance) contributed between 48 and 74% of the July-September streamflow, but
837 did not provide annual values due to the lack of streamflow measurements in other months. For the highly
838 glacierized Nordic Creek basin (58% glacier-cover in 2013), Moore *et al.* (2020), found that the wastage
839 flux contributed from 9-19% of annual water yield, much lower values than calculated in this study.
840 Further comparison can be made with modelling studies of alpine glacierized basin in other mountain
841 ranges, but caution is needed in interpreting these for comparison due to the difference in climate and
842 modelling methodology. In the Alps, Verbunt *et al.* (2003) found that in a 47% glacierized basin, the glacier
843 runoff (snow, and ice melt, but not rainfall on the glacier) contributed 62% of total streamflow, with 20%
844 originating from ice melt, 10% from firn melt and 32% from on-glacier snowmelt, but did not indicate the
845 proportion of off-glacier snowmelt contribution to streamflow and therefore underestimated the
846 contribution of snowmelt at the basin scale. The same study also found that for a basin with 69% glacier
847 cover, the glacier runoff contributed 85% of basin streamflow. Gao *et al.* (2012) found that, in a 44%
848 glacierized basin in Central Asia, 60% of the basin streamflow originated from the glacierized area, which
849 includes firn, snow and ice melt and liquid routed on the glacier surface. These proportions of on-glacier
850 runoff contribution to streamflow are comparable to the results from the PGRB, where 71% of annual
851 runoff originates from the glacier area (including firn melt, snowmelt, ice melt and rainfall on the glacier),
852 which covers 56% of the basin. In the Andes, Burger *et al.* (2019) found that in a basin with 16% glacier
853 cover, snowmelt on and off the glacier contributed 66-93% of basin streamflow, ice melt formed 3.5-32%,
854 and rainfall-runoff did not exceed 6%. Therefore, the numbers presented here are within the ranges of
855 values obtained in highly glacierized alpine basins, but the different approaches to computing flow

856 compositions and glacier runoff contribution to streamflow preclude deeper comparisons between
857 different studies. To facilitate future comparison between hydrological studies in mountain basins, the
858 glacio-hydrological community should define common and clear metrics to compare runoff components,
859 including both on and off-glacier runoff components and glacier wastage contributions to streamflow.

860

861 **5. CONCLUSIONS**

862 Streamflow generation in a glacierized mountain catchment such as the PGRB is caused by a complex
863 interplay of hydrological processes. This study aimed to investigate the key sources of inter-annual
864 streamflow variability in a highly glacierized basin. To do so, a process-oriented, physically based glacier
865 hydrological model was created in the Cold Regions Hydrological Modelling Platform to represent the full
866 range of processes generating streamflow in a small glacierized Canadian Rockies headwater basin for the
867 period 1990-2020. By using parameters derived from fieldwork, literature values or physical principles,
868 the model was able to capture the basin's snow accumulation, ice and snow melt patterns, and
869 streamflow well. These modelling results emphasise the importance of long-term in-situ observations of
870 meteorological variables in remote, high altitude glacierized basin to guide and evaluate model
871 application.

872

873 Even though trends were obtained in selected meteorological forcings in the PGRB (summer air
874 temperature, summer and annual rainfall and winter snowfall), these trends did not translate into trends
875 in streamflow or runoff components. The predominance of interannual variability in the glacierized basin
876 streamflow was due to hydrometeorological factors that affected ice melt with much smaller impacts
877 from firn melt and rainfall-runoff. Annual streamflow was significantly correlated with annual air
878 temperature, as well as summer rainfall and winter snowfall. The negative correlation with winter
879 snowfall and with timing of ice exposure, concomitant with the lack of association between snowmelt and
880 streamflow indicates that winter conditions play a role in streamflow variability by regulating subsequent
881 summer ice exposure and albedo in the PGRB. Lower snowfall reduces summer albedo on the glacier.
882 Snowmelt, whilst generating a larger fraction of streamflow, was a small source of interannual streamflow
883 variability because high snowfall years were also low ice melt years due to the impact of deep snowpack
884 in covering and protecting glacier ice from melting until late in the summer.

885

886 A comparison of high and low streamflow years showed that streamflow in high flow years was 41%
887 greater than in low flow years. High flow years were warmer (+1.43 °C), rainier (+145 mm) and less snowy
888 (-295 mm w.e.) than low flow years. These differences in temperature and precipitation caused earlier
889 snowmelt (-10 days), enhanced ice melt (+103%) and firn melt (+162%), and greater rainfall-runoff
890 (+146%). As low snowfall years were warmer and rainier years than high snowfall years, rainfall and firn
891 melt runoff sources also increased with ice melt in these years. High snowfall did not necessarily translate
892 into high snowmelt, as in high snowfall years not all the snow melted. These compensatory feedbacks
893 between snow and glacier runoff processes affected both interannual variability and long-term trends.
894 This assessment of trends in the PGRB combined with an analysis of the correlation between
895 meteorological conditions and streamflow and a diagnosis of the hydrometeorological conditions
896 resulting in high and low flow years revealed the key drivers of streamflow variability in the PGRB but also
897 highlighted the complexities of streamflow generation in mountain catchments.

898
899 Considering that meteorological extremes are expected to increase in the future, and that glacier retreat
900 enhances flow variability by changing the streamflow regime from ice-dominated to snowmelt and
901 rainfall-runoff dominated, the streamflow in headwater glacierized basins is expected to continue to
902 change in the upcoming decades. Increasingly warm conditions may cause an increase in the frequency
903 of high flow conditions whilst glacier coverage still remains, much as was noted in the shift from the 1960s
904 to recent years by Pradhananga and Pomeroy (2022a). These future changes will be superimposed on the
905 current inter-annual variability that currently dominates the streamflow response in the PGRB. To
906 understand and robustly predict the changing water supply from in glacierized mountain basins, it is
907 crucial to consider the complex interplay of streamflow generation processes.

908
909 **6. ACKNOWLEDGEMENTS**
910 The authors wish to thank the Natural Sciences Engineering and Research Council of Canada Discovery
911 Grants and Vanier and Michael Smith Scholarships, the Canada Foundation for Innovation, Canada
912 Research Chairs programme and the Canada First Research Excellence Fund's Global Water Futures
913 programme for support. Peyto Glacier Research Basin has been maintained by many people over the
914 years including most recently, Mike Demuth and Mark Ednie of Natural Resources Canada, and May Guan,
915 Angus Duncan, Eric Courtin and Greg Galloway of the Centre for Hydrology, University of Saskatchewan.
916 We thank Dan Moore and an additional reviewer for their helpful and thorough comments on the
917 manuscript.
918

919 **APPENDIX A**

920 **Table A1. Geomorphic characteristics of the CRHM hydrological response units (HRUs). The HRU**
 921 **number are found on Fig. 1b. The cover-type refer to the landscape at the beginning of the**
 922 **simulation, and the land cover type in parenthesis refer to the landscape in 2015.**

HRU number	Elevation (m)	Area (km ²)	Slope (°)	Aspect (°)	Cover Type
1	2949	0.3231	29.53	40	Glacier
2	2802	1.786	15.91	40	Glacier
3	2701	0.2819	5.203	344	Glacier
4	2654	0.8719	12.33	344	Glacier
5	2560	1.459	14.05	3	Glacier
6	2449	0.8744	8.181	352	Glacier
7	2252	0.3325	7.438	27	Glacier
8	2211	0.2331	4.749	350	Glacier (Moraine)
9	2176	0.2971	6.566	350	Glacier (Moraine)
10	2141	0.0863	13.96	307	Moraine
11	2956	0.2594	29.35	67	Glacier
12	2799	1.104	15.19	67	Glacier
13	2660	0.9737	15.33	60	Glacier
14	2552	0.3394	12.98	40	Glacier
15	2460	0.2731	10.9	75	Glacier
16	2405	0.2081	10.4	72	Glacier (Steep talus)
17	2251	0.0719	10.68	15	Debris-cover
18	2705	0.5981	20.14	84	Glacier
19	2545	0.3425	14.01	121	Glacier
20	2445	0.2275	10.06	111	Glacier (Moraine)
21	2200	0.1306	7.914	40	Debris-cover (Moraine)
22	2741	0.965	26.63	184	Steep talus
23	2501	0.7519	16.57	180	Moraine
24	2554	0.6163	43.62	103	Cliff
25	2273	0.4619	19.19	118	Ice-cored moraine
26	2215	0.26	14.16	145	Moraine
27	2771	1.395	27.97	250	Steep talus
28	2502	0.5512	13.54	256	Moraine
29	2285	0.4463	25.06	305	Ice-cored moraine
30	2702	0.4806	44.91	326	Cliff
31	2533	0.4644	26.58	287	Moraine
32	2375	0.9269	18.38	278	Moraine
33	2393	0.1144	8.185	33	Debris-cover
34	2413	0.1912	7.622	7	Glacier
35	2482	0.09313	24.17	70	Cliff
36	2727	0.35	30.54	80	Cliff
37	2847	0.2625	38.12	4	Cliff

923

924

925 **APPENDIX B**

926 Glacier melt contributions to streamflow are divided between melt and wastage following Comeau *et al.*
927 (2009), with wastage corresponding to net glacier volume loss resulting from negative mass balance and
928 melt referring to a storage term from snowfall and snowmelt. A key difference is the inclusion of the firn
929 melt component to the glacier ice melt calculations.

930 In years of positive or neutral mass balance, the glacier ice and firn melt is lower than the leftover snowfall
931 at the end of the melt season, and no wastage occurs. During these years, the melt component equals to
932 the ice melt M_i .

933
934
$$M_i + M_f \leq P_s - M_s, \quad Wastage = 0, \quad Melt = M_i$$

935 Where M_i is the glacier ice melt, M_f is the glacier firn melt, P_s is the snowfall over the glacier area, and M_s
936 is the snowmelt over the glacier area.

937 In years with negative mass balance, the ice and firn melt from the glacier area is larger than the residual
938 snowfall at the end of the melt season:

939
$$M_i + M_f > P_s - M_s$$

940
$$Wastage = (M_i + M_f) - (P_s - M_s)$$

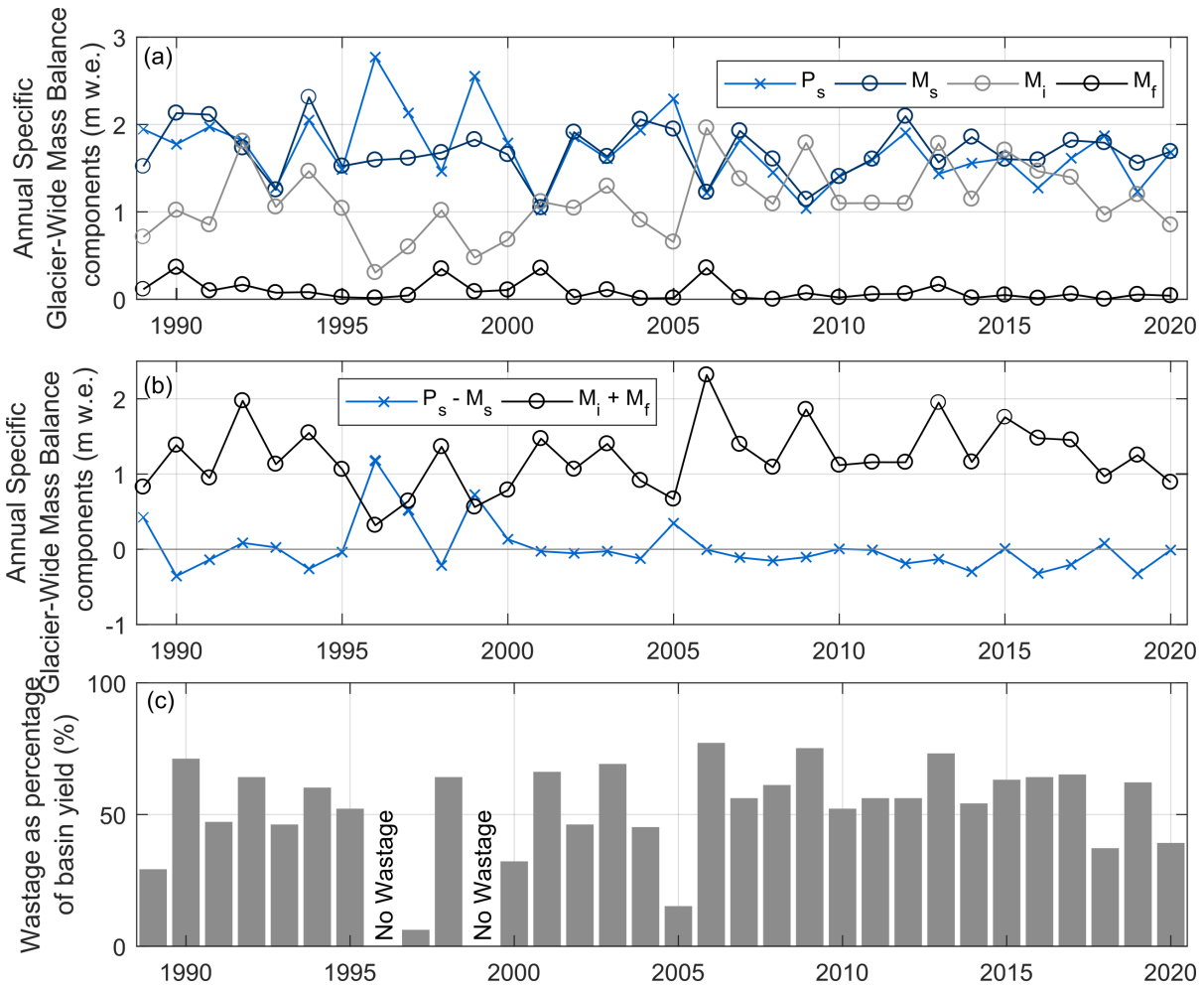
941
$$Melt = P_s - M_s$$

942 In years of negative mass balance, wastage is defined as the volume of ice and firn melt that exceeds the
943 water equivalent volume of snow accumulation into the glacier.

944 The percentage of glacier wastage contribution to streamflow is calculated as a percentage of the annual
945 basin yield, defined as the combination of streamflow simulated at the basin outlet and groundwater
946 discharge from the basin.

947 The individual components of the wastage calculation are shown in Fig. B.1. In the case of Peyto, due to
948 both rain-on-snow events and snow redistribution from blowing snow and avalanches, the glacier area
949 snowmelt (M_s) is slightly larger than the glacier area snowfall (P_s) for 21 out of the 32 years analyzed. In
950 these 21 years, the snowmelt is on average 10% higher than the snowfall across the glacier, with a
951 maximum difference of 27%.

952 Of the 32 years simulated, only two years do not have a wastage component, due to showing a positive
953 mass balance with the ice melt component being smaller or equal to the snow remaining on the glacier at
954 the end of the hydrological year ($P_s - M_s$). For the 30 years with wastage, the wastage volume was
955 calculated as a ratio to the total basin yield (combined streamflow and groundwater), and contributed
956 between 6% and 77% of basin yield, and averaging 53%.



957

958 **Figure B1. Annual specific mass-balance components for the Peyto Glacier for years 1988-2020, with**
 959 **annual snowfall (P_s), snow melt (M_s), ice melt (M_i) and firn melt (M_f) in (a), the combined snow**
 960 **components ($P_s - M_s$) and glacier ice and firn ($M_i + M_f$) and the wastage as a proportion of annual basin**
 961 **yield in (c).**

962

963 **REFERENCES**

- 964 Aubry-Wake C, Lamontagne-Hallé P, Baraër M, McKenzie JM, Pomeroy JW. 2022. Using ground-based
965 thermal imagery to estimate debris thickness over glacial ice: Fieldwork considerations to improve
966 the effectiveness. *Journal of Glaciology*, 1-17 DOI:10.1017/jog.2022.67
- 967 Ayers HD. 1959. Influence of soil profile and vegetation characteristic on net rainfall supply to runoff. In
968 *Spillway Design Floods: Proceeding of Hydrology Symposium No. 1, National Research Council of*
969 *Canada*. 198–205.
- 970 Beniston M. 2003. Climatic change in mountain regions: A review of possible impacts. In *Climatic*
971 *Change*. Kluwer Academic Publishers; 5–31. DOI: 10.1023/A:1024458411589
- 972 Benn DI, Evans DJA. 2010. *Glaciers and Glaciation* (2nd Edition). Routledge.
- 973 Bernhardt M, Schulz K. 2010. SnowSlide: A simple routine for calculating gravitational snow transport.
974 *Geophysical Research Letters* **37** (11) DOI: 10.1029/2010GL043086
- 975 Bernhardt M, Schulz K, Liston GE, Zängl G. 2012. The influence of lateral snow redistribution processes
976 on snow melt and sublimation in alpine regions. *Journal of Hydrology* **424–425**: 196–206 DOI:
977 10.1016/j.jhydrol.2012.01.001
- 978 Beven K. 2016. Facets of uncertainty: E
979 pistemic uncertainty, non-stationarity, likelihood, hypothesis testing, and communication. *Hydrological*
980 *Sciences Journal* **61** (9): 1652–1665 DOI: 10.1080/02626667.2015.1031761
- 981 Burger F, Ayala A, Farias D, Shaw TE, MacDonell S, Brock B, McPhee J, Pellicciotti F. 2019. Interannual
982 variability in glacier contribution to runoff from a high-elevation Andean catchment: understanding
983 the role of debris cover in glacier hydrology. *Hydrological Processes* **33** (2): 214–229 DOI:
984 10.1002/HYP.13354
- 985 Campbell ÉMS, Ryan MC. 2021. Nested recharge systems in mountain block hydrology: high-elevation
986 snowpack generates low-elevation overwinter baseflow in a Rocky Mountain river. *Water* **13** (16):
987 2249 DOI: 10.3390/W13162249
- 988 Carenzo M, Pellicciotti F, Mabilard J, Reid T, Brock BW. 2016. An enhanced temperature index model for
989 debris-covered glaciers accounting for thickness effect. *Advances in Water Resources* **94**: 457–469
990 DOI: 10.1016/j.advwatres.2016.05.001
- 991 Castellazzi P, Burgess D, Rivera A, Huang J, Longuevergne L, Demuth MN. 2019. Glacial melt and
992 potential impacts on water resources in the Canadian Rocky Mountains. *Water Resources Research*
993 **55** (12): 10191–10217 DOI: 10.1029/2018WR024295
- 994 Chen J, Ohmura A. 1990. Estimation of Alpine glacier water resources and their change since the 1870s.
995 IAHS Publications 193: 127–135.
- 996 Clark, CO. 1945. Storage and the unit hydrograph, Proc. Am. Soc. Civil Eng., 69, 1419–1447.
- 997 Clark MP, Wilby RL, Gutmann ED, Vano JA, Gangopadhyay S, Wood AW, Fowler HJ, Prudhomme C,
998 Arnold JR, Brekke LD. 2016. Characterizing uncertainty of the hydrologic impacts of climate change.
999 *Current Climate Change Reports* **2** (2): 55–64 DOI: 10.1007/S40641-016-0034-X/FIGURES/1
- 1000 Clow DW, Schrott L, Webb R, Campbell DH, Torizzo A, Dornblaser M. 2003. Ground water occurrence
1001 and contributions to streamflow in an alpine catchment, Colorado Front Range. *Groundwater* **41**
1002 (7): 937–950 DOI: 10.1111/j.1745-6584.2003.tb02436.x
- 1003 Comeau L, Pietroniro A, Demuth MN. 2009. Glacier contribution to the North and South
1004 Saskatchewan Rivers. *Hydrological Processes* **23** (18): 2640–2653 DOI: 10.1002/hyp
- 1005 DeBeer CM, Pomeroy JW. 2009. Modelling snow melt and snowcover depletion in a small alpine cirque,
1006 Canadian Rocky Mountains. *Hydrological Processes* **23** (18): 2584–2599 DOI: 10.1002/hyp.7346
- 1007 DeBeer CM, Wheeler HS, Carey SK, Chun KP. 2016. Recent climatic, cryospheric, and hydrological
1008 changes over the interior of western Canada: a review and synthesis. *Hydrol. Earth Syst. Sci* **20** (4):
1009 1573–1598 DOI: 10.5194/hess-20-1573-2016
- 1010 Dee DP, Uppala SM, Simmons AJ, Berrisford P, Poli P, Kobayashi S, Andrae U, Balmaseda MA, Balsamo G,

1011 Bauer P, et al. 2011. The ERA-Interim reanalysis: Configuration and performance of the data
1012 assimilation system. *Quarterly Journal of the Royal Meteorological Society* **137** (656): 553–597 DOI:
1013 10.1002/qj.828

1014 Demuth MN, Keller R. 2006. An assessment of the mass balance of Peyto glacier (1966-1995) and its
1015 relation to Recent and past-century climatic variability. In *Peyto Glacier: One Century of Science*,
1016 Demuth, M.N. DSM and GJY (ed.).National Hydrology Research Institute Science Report 8; 83–132.

1017 Demuth MN, Munro DS, Young GJ. 2006. *Peyto Glacier : one century of science*. National Hydrology
1018 Research Institute, Saskatoon, Saskatchewan

1019 Duethmann D, Bloschl G, Parajka J. 2020. Why does a conceptual hydrological model fail to correctly
1020 predict discharge changes in response to climate change? *Hydrology and Earth System Sciences* **24**
1021 (7): 3493–3511 DOI: 10.5194/HESS-24-3493-2020

1022 Dyurgerov MB. 2002. Glacier mass balance and regime: data of measurement and analysis. Institute of
1023 Arctic and Alpine Research. *Occasional Paper 55, University of Colorado, Boulder* **55**: 1–268

1024 Essery R, Etchevers P. 2004. Parameter sensitivity in simulations of snowmelt. *Journal of Geophysical*
1025 *Research* **109** (D20111): 1–15 DOI: 10.1029/2004JD005036

1026 Fan Y. 2019. Are catchments leaky? *WIRES Water* **6** (6) DOI: 10.1002/wat2.1386

1027 Fang X, Pomeroy JW, Ellis CR, MacDonald MK, DeBeer CM, Brown T. 2013. Multi-variable evaluation of
1028 hydrological model predictions for a headwater basin in the Canadian Rocky Mountains. *Hydrology*
1029 *and Earth System Sciences* **17** (4): 1635–1659 DOI: 10.5194/hess-17-1635-2013

1030 Farinotti D, Usselman S, Huss M, Bauder A, Funk M. 2012. Runoff evolution in the Swiss Alps:
1031 projections for selected high-alpine catchments based on ENSEMBLES scenarios. *Hydrological*
1032 *Processes* **26** (13): 1909–1924 DOI: 10.1002/hyp.8276

1033 Fountain AG, Tangborn W V. 1985. The Effect of glaciers on streamflow variations. **21** (4): 579–586 DOI:
1034 10.1029/WR021i004p00579

1035 Frans C, Istanbuluoglu E, Lettenmaier DP, Fountain AG, Riedel J. 2018. Glacier recession and the
1036 response of summer streamflow in the Pacific Northwest United States, 1960–2099. *Water*
1037 *Resources Research* **54** (9): 6202–6225 DOI: 10.1029/2017WR021764

1038 Frenierre JL La, Mark BG, La Frenierre J, Mark BG, Frenierre JL La, Mark BG. 2013. A review of methods
1039 for estimating the contribution of glacial meltwater to total watershed discharge. *Progress in*
1040 *Physical Geography* **38** (2): 173–200 DOI: 10.1177/0309133313516161

1041 Freudiger D, Kohn I, Seibert J, Stahl K, Weiler M. 2017. Snow redistribution for the hydrological modeling
1042 of alpine catchments. *Wiley Interdisciplinary Reviews: Water* **4** (5): e1232 DOI: 10.1002/wat2.1232

1043 Fyffe CL, Brock BW, Kirkbride MP, Mair DWF, Arnold N, Smiraglia C, Diolaiuti G, Diotri F. 2019a. Do
1044 debris-covered glaciers demonstrate distinctive hydrological behaviour compared to clean glaciers?
1045 *Journal of Hydrology* **570**, 584–597. DOI: <https://doi.org/10.1016/j.jhydrol.2018.12.069>

1046 Fyffe, C. L., Brock, B. W., Kirkbride, M. P., Black, A. R., Smiraglia, C., & Diolaiuti, G. 2019b. The impact of
1047 supraglacial debris on proglacial runoff and water chemistry. *Journal of Hydrology* **576**, 41–57.
1048 <https://doi.org/10.1016/J.JHYDROL.2019.06.023>

1049 Gao H, He X, Ye B, Pu J. 2012. Modeling the runoff and glacier mass balance in a small watershed on the
1050 Central Tibetan Plateau, China, from 1955 to 2008. *Hydrological Processes* **26** (11): 1593–1603 DOI:
1051 10.1002/hyp.8256

1052 Garnier B, Ohmura A. 1970. The evaluation of surface variations in solar radiation income. *Solar Energy*
1053 **13**: 21–34 DOI:10.1016/0038-092X(70)90004-6

1054 Garrick M, Cunnane C, Nash JE. 1978. A criterion of efficiency for rainfall-runoff models. *Journal of*
1055 *Hydrology* DOI: 10.1016/0022-1694(78)90155-5

1056 Gibbons JD, Chakraborti S. 2010. *Nonparametric statistical inference*. Chapman and Hall/CRC. DOI:
1057 10.5005/jp/books/10313_14

1058 Gray DM, Toth B, Zhao L, Pomeroy JW, Granger RJ. 2001. Estimating areal snowmelt infiltration into

1059 frozen soils. *Hydrological Processes* **15** (16): 3095–3111 DOI: 10.1002/hyp.320

1060 Grisogono B, Oerlemans J. 2001. A theory for the estimation of surface fluxes in simple katabatic flows.

1061 *Quarterly Journal of the Royal Meteorological Society* **127** (578): 2725–2739 DOI:

1062 10.1002/qj.49712757811

1063 Gruber S, Haeberli W. 2009. Mountain Permafrost. In *Permafrost Soils* Springer Berlin Heidelberg: Berlin,

1064 Heidelberg; 33–44. DOI: 10.1007/978-3-540-69371-0_3

1065 Gupta H V, Kling H, Yilmaz KK, Martinez GF. 2009. Decomposition of the mean squared error and NSE

1066 performance criteria: Implications for improving hydrological modelling. *Journal of Hydrology* **377**

1067 (1–2): 80–91 DOI: 10.1016/j.jhydrol.2009.08.003

1068 Hanzer F, Helfricht K, Marke T, Strasser U. 2016. Multilevel spatiotemporal validation of snow/ice mass

1069 balance and runoff modeling in glacierized catchments. *Cryosphere* **10** (4): 1859–1881 DOI:

1070 10.5194/TC-10-1859-2016

1071 Harder P, Pomeroy JW. 2013. Estimating precipitation phase using a psychrometric energy balance

1072 method. *Hydrological Processes* **27** (May): 1901–1914 DOI: 10.1002/hyp.9799

1073 Harder P, Pomeroy JW, Westbrook CJ. 2015. Hydrological resilience of a Canadian Rockies headwaters

1074 basin subject to changing climate, extreme weather, and forest management. *Hydrological*

1075 *Processes* **29** (18): 3905–3924 DOI: 10.1002/hyp.10596

1076 Hayashi M. 2020. Alpine Hydrogeology: The critical role of groundwater in sourcing the headwaters of

1077 the wGorld. *Groundwater* **58** (4): 498–510 DOI: 10.1111/GWAT.12965

1078 Henn B, Newman AJ, Livneh B, Daly C, Lundquist JD. 2018. An assessment of differences in gridded

1079 precipitation datasets in complex terrain. *Journal of Hydrology* **556**: 1205–1219 DOI:

1080 10.1016/J.JHYDROL.2017.03.008

1081 Hock R. 1999. A distributed temperature-index ice- and snowmelt model including potential direct solar

1082 radiation. *Journal of Glaciology* **45** (149): 101–111 DOI: 10.1017/S0022143000003087

1083 Hock R. 2005. Glacier melt: a review of processes and their modelling. *Progress in Physical Geography* **29**

1084 (3): 362–391 DOI: 10.1191/0309133305pp453ra

1085 Hock R, Noetzli C. 1997. Areal Melt and Discharge Modelling of Storglaciären, Sweden. *Annals of*

1086 *Glaciology* **24**: 211–16. DOI: 10.1017/s0260305500012192.

1087 Hood JL, Hayashi M. 2015. Characterization of snowmelt flux and groundwater storage in an alpine

1088 headwater basin. *Journal of Hydrology* **521**: 482–497 DOI: 10.1016/j.jhydrol.2014.12.041

1089 Hopkinson C, Young GJ. 1998. The effect of glacier wastage on the flow of the Bow River at Banff,

1090 Alberta, 1951–1993. *Hydrological Processes* **12** (10–11): 1745–1762 DOI: 10.1002/(SICI)1099-

1091 1085(199808/09)12:10/11<1745::AID-HYP692>3.0.CO;2-S

1092 Hopkinson C, Demuth MN, Sitar M. 2012. Hydrological implications of periglacial expansion in the Peyto

1093 Glacier catchment, Canadian Rockies. International Association for the Hydrological Sciences/*IUGG*

1094 *Redbook Publication* 352, p.341–344

1095 Houze RA. 2012. Orographic effects on precipitating clouds. *Reviews of Geophysics* **50** (1): 1001 DOI:

1096 10.1029/2011RG000365

1097 Hugonnet R, McNabb R, Berthier E, Menounos B, Nuth C, Girod L, Farinotti D, Huss M, Dussailant I, Brun

1098 F, et al. 2021. Accelerated global glacier mass loss in the early twenty-first century. *Nature* **592**

1099 (7856): 726–731 DOI: 10.1038/s41586-021-03436-z

1100 Huss M, Bookhagen B, Huggel C, Jacobsen D, Bradley RSS, Clague JJJ, Vuille M, Buytaert W, Cayan DRR,

1101 Greenwood G, et al. 2017. Toward mountains without permanent snow and ice. *Earth's Future* **5**

1102 (5): 418–435 DOI: 10.1002/2016EF000514

1103 Immerzeel WW, van Beek LPH, Bierkens MFP. 2010. Climate change will affect the asian water towers.

1104 *Science* **328** (5984): 1382–1385 DOI: 10.1126/science.1183188

1105 Jansson P, Hock R, Schneider T. 2003. The concept of glacier storage: A review. *Journal of Hydrology* **282**

1106 (1–4): 116–129 DOI: 10.1016/S0022-1694(03)00258-0

1107 Jost G, Moore RD, Menounos B, Wheate R. 2012. Quantifying the contribution of glacier runoff to
1108 streamflow in the upper Columbia River Basin, Canada. *Hydrology and Earth System Sciences* **16** (3):
1109 849–860 DOI: 10.5194/hess-16-849-2012

1110 Kirchner JW. 2006. Getting the right answers for the right reasons: Linking measurements, analyses, and
1111 models to advance the science of hydrology. *Water Resources Research* **42** (3) DOI:
1112 10.1029/2005WR004362

1113 Knoben WJM, Freer JE, Woods RA. 2019. Technical note: Inherent benchmark or not? Comparing Nash-
1114 Sutcliffe and Kling-Gupta efficiency scores. *Hydrology and Earth System Sciences* **23** (10): 4323–
1115 4331 DOI: 10.5194/hess-23-4323-2019

1116 Koboltschnig GR, Schöner W. 2011. The relevance of glacier melt in the water cycle of the Alps: the
1117 example of Austria. *Hydrology and Earth System Sciences* **15** (6): 2039–2048 DOI: 10.5194/hess-15-
1118 2039-2011

1119 Krogh SA, Pomeroy JW, McPhee J. 2015. Physically based mountain hydrological modeling using
1120 reanalysis data in Patagonia. *Journal of Hydrometeorology* **16** (1): 172–193 DOI: 10.1175/JHM-D-13-
1121 0178.1

1122 Langston G, Bentley LR, Hayashi M, McClymont AF, Pidlisecky A. 2011. Internal structure and
1123 hydrological functions of an alpine proglacial moraine. *Hydrological Processes* **25**: 2967–2982 DOI:
1124 10.1002/hyp.8144

1125 Van Loon AF, Ploum SW, Parajka J, Fleig AK, Garnier E, Laaha G, Van Lanen HAJ. 2015. Hydrological
1126 drought types in cold climates: Quantitative analysis of causing factors and qualitative survey of
1127 impacts. *Hydrology and Earth System Sciences* **19** (4): 1993–2016 DOI: 10.5194/hess-19-1993-2015

1128 López-Moreno J-I, Gascoïn S, Herrero J, Sproles EA, Pons M, Alonso-González E, Hanich L, Boudhar A,
1129 Musselman KN, Molotch NP, et al. 2017. Different sensitivities of snowpacks to warming in
1130 Mediterranean climate mountain areas. *Environmental Research Letters* **12** (7): 74006 DOI:
1131 10.1088/1748-9326/aa70cb

1132 López-Moreno J-I, Pomeroy JW, Alonso-González E, Morán-Tejeda E, Revuelto-Benedí J, Revuelto J.
1133 2020. Decoupling of warming mountain snowpacks from hydrological regimes. *Environmental*
1134 *Research Letters* **15** (11): 114006 DOI: 10.1088/1748-9326/abb55f

1135 Lundquist JD, Hughes M, Henn B, Gutmann ED, Livneh B, Dozier J, Neiman P. 2015. High-Elevation
1136 Precipitation Patterns: Using Snow Measurements to Assess Daily Gridded Datasets across the
1137 Sierra Nevada, California. *Journal of Hydrometeorology* **16** (4): 1773–1792 DOI: 10.1175/JHM-D-15-
1138 0019.1

1139 MacDonald MK, Pomeroy JW, Pietroniro A. 2009. Parameterizing redistribution and sublimation of
1140 blowing snow for hydrological models: Tests in a mountainous subarctic catchment. *Hydrological*
1141 *Processes* **23** (18): 2570–2583 DOI: 10.1002/hyp.7356

1142 MacDonald MK, Pomeroy JW, Pietroniro A. 2010. On the importance of sublimation to an alpine snow
1143 mass balance in the Canadian Rocky Mountains. *Hydrology and Earth System Sciences* **14** (7): 1401–
1144 1415 DOI: 10.5194/hess-14-1401-2010

1145 Marks D, Domingo J, Susong D, Link TE, Garen D. 1999. A spatially distributed energy balance snowmelt
1146 model for application in mountain basins. *Hydrological Processes* **13** (12–13): 1935–1959 DOI:
1147 10.1002/(SICI)1099-1085(199909)13:12/13<1935::AID-HYP868>3.0.CO;2-C

1148 McClung DM, Schaerer PA. 2006. *The avalanche handbook*. Mountaineers Books. DOI:
1149 10.5860/choice.31-3797

1150 McClymont AF, Hayashi M, Bentley LR, Muir D, Ernst E. 2010. Groundwater flow and storage within an
1151 alpine meadow-talus complex. *Hydrology and Earth System Sciences* **14** (6): 859–872 DOI:
1152 10.5194/hess-14-859-2010

1153 Milner AM, Khamis K, Battin TJ, Brittain JE, Barrand NE, Füreder L, Cauvy-Fraunié S, Gíslason GM,
1154 Jacobsen D, Hannah DM, et al. 2017. Glacier shrinkage driving global changes in downstream

1155 systems. *Proceedings of the National Academy of Sciences of the United States of America* **114** (37):
1156 9770–9778 DOI: 10.1073/pnas.1619807114

1157 Moore RD, Pelto B, Menounos B, Hutchinson D. 2020. Detecting the effects of sustained glacier wastage
1158 on streamflow in variably glacierized catchments. *Frontiers in Earth Science* **8** (May): 136 DOI:
1159 10.3389/feart.2020.00136

1160 Muir DL, Hayashi M, Mcclymont AF. 2011. Hydrological storage and transmission characteristics of an
1161 alpine talus. *Hydrological Processes* **25** (19): 2954–2966 DOI: 10.1002/hyp.8060

1162 Munro DS. 1989. Surface roughness and bulk heat transfer on a glacier: comparison with eddy
1163 correlation. *Journal of Glaciology* **35** (121): 343–348 DOI: 10.3189/S0022143000009266

1164 Munro DS. 2004. Revisiting bulk heat transfer on Peyto Glacier, Alberta, Canada, in light of the OG
1165 parameterization. *Journal of Glaciology* **50** (171): 590–600 DOI: 10.3189/172756504781829819

1166 Munro DS. 2011. Delays of supraglacial runoff from differently defined microbasin areas on the Peyto
1167 Glacier. *Hydrological Processes*: n/a-n/a DOI: 10.1002/hyp.8124

1168 Munro DS. 2013. Creating a runoff record for an ungauged basin: Peyto Glacier, 2002-2007. In *Putting*
1169 *Prediction in Ungauged Basins into Practice* 197–204.

1170 Naz BS, Frans C, Clarke G, Burns P, Lettenmaier DP. 2014. Modeling the effect of glacier recession on
1171 streamflow response using a coupled glacio-hydrological model. *Hydrol. Earth Syst. Sci* **18**: 787–802
1172 DOI: 10.5194/hess-18-787-2014

1173 Nienow P, Sharp M, Willis I. 1998. Seasonal changes in the morphology of the subglacial drainage
1174 system, Haut Glacier d'Arolla, Switzerland. *Earth Surf. Process. Landforms* **23**: 825-843. DOI:
1175 [https://doi.org/10.1002/\(SICI\)1096-9837\(199809\)23:9<825::AID-ESP893>3.0.CO;2-2](https://doi.org/10.1002/(SICI)1096-9837(199809)23:9<825::AID-ESP893>3.0.CO;2-2)

1176 Ommanney, C. S. L. 2002. Glaciers of the Canadian Rockies. In R. S. Williams, & J. G. Ferrigno (Eds.),
1177 Satellite Image Atlas of the Glaciers of the World — North America (pp. J199–J289). U.S. Geological
1178 Survey Professional Paper 1386-J-1.

1179 Østrem G, Arnold K, Ostrem G. 1970. Ice-Cored Moraines in Southern British Columbia and Alberta,
1180 Canada. *Geografiska Annaler. Series A, Physical Geography* **52** (2): 120 DOI: 10.2307/520605

1181 Pellicciotti F, Buergi C, Immerzeel WW, Konz M, Shrestha AB. 2012. Challenges and uncertainties in
1182 hydrological modeling of remote Hindu Kush–Karakoram–Himalayan (HKH) basins: Suggestions for
1183 calibration strategies. *Mountain Research and Development* **32** (1): 39–50 DOI: 10.1659/MRD-
1184 JOURNAL-D-11-00092.1

1185 Pepin NC, Arnone E, Gobiet A, Haslinger K, Kotlarski S, Notarnicola C, Palazzi E, Seibert P, Serafin S,
1186 Schöner W, et al. 2022. Climate changes and their elevational patterns in the mountains of the
1187 World. *Reviews of Geophysics* **60** (1) DOI: 10.1029/2020rg000730

1188 Pomeroy JW, Li L. 2000. Prairie and arctic areal snow cover mass balance using a blowing snow model.
1189 *Journal of Geophysical Research: Atmospheres* **105** (D21): 26619–26634 DOI:
1190 10.1029/2000JD900149

1191 Pomeroy JW, Fang X, Shook K, Whitfield PH. 2013. Predicting in ungauged basins using physical
1192 principles obtained using the deductive, inductive, and abductive reasoning approach. In *Putting*
1193 *Predictions in Ungauged Basins into Practice* 41–62.

1194 Pomeroy JW, Gray DM, Brown T, Hedstrom NR, Quinton WL, Granger RJ, Carey SK. 2007. The cold
1195 regions hydrological model: A platform for basing process representation and model structure on
1196 physical evidence. *Hydrological Processes* **21** (19): 2650–2667 DOI: 10.1002/hyp.6787

1197 Pomeroy JW, Gray DMM, Landline PG, Landine PG. 1993. The Prairie Blowing Snow Model:
1198 characteristics, validation, operation. *Journal of Hydrology* **144** (1–4): 165–192 DOI: 10.1016/0022-
1199 1694(93)90171-5

1200 Pomeroy JW, Marsh P, Gray DM. 1997. Application of a distributed blowing snow model to the Arctic.
1201 *Hydrological Processes* **11** (11): 1451–1464 DOI: 10.1002/(SICI)1099-1085(199709)11:11<1451::AID-
1202 HYP449>3.0.CO;2-Q

1203 Pradhananga D, Pomeroy JW. 2022a. Recent hydrological response of glaciers in the Canadian Rockies to
1204 changing climate and glacier configuration. *Hydrol. Earth Syst. Sci* **26**: 2605–2616 DOI:
1205 10.5194/hess-26-2605-2022

1206 Pradhananga D, Pomeroy JW. 2022b. Diagnosing changes in glacier hydrology from physical principles
1207 using a hydrological model with snow redistribution, sublimation, firnification and energy balance
1208 ablation algorithms. *Journal of Hydrology* **608**: 127545 DOI: 10.1016/j.jhydrol.2022.127545

1209 Pradhananga D, Pomeroy JW, Aubry-Wake C, Munro DS, Shea J, Demuth MN, Kirat NH, Menounos B,
1210 Mukherjee K. 2021. Hydrometeorological, glaciological and geospatial research data from the Peyto
1211 Glacier Research Basin in the Canadian Rockies. *Earth System Science Data* **13** (6): 2875–2894 DOI:
1212 10.5194/essd-13-2875-2021

1213 Radic V, Hock R. 2014. Glaciers in the Earth’s hydrological cycle: Assessments of glacier mass and runoff
1214 changes on global and regional scales. *Surveys in Geophysics* **35** (3): 813–837 DOI: 10.1007/s10712-
1215 013-9262-y

1216 Rasouli K, Pomeroy JW, Janowicz JR, Carey SK, Williams TJ. 2014. Hydrological sensitivity of a northern
1217 mountain basin to climate change. *Hydrological Processes* **28** (14) DOI: 10.1002/hyp.10244

1218 Reid T, Brock BW. 2010. An energy-balance model for debris-covered glaciers including heat conduction
1219 through the debris layer. *Journal of Glaciology* **56** (199): 903–916 DOI:
1220 10.3189/002214310794457218

1221 Saberi L, Mclaughlin RT, Ng G-HC, Frenierre J La, Wickert AD, Baraer M, Zhi W, Li L, Mark BG. 2019.
1222 Multi-scale temporal variability in meltwater contributions in a tropical glacierized watershed.
1223 *Hydrol. Earth Syst. Sci* **23**: 405–425 DOI: 10.5194/hess-23-405-2019

1224 Schaefli B, Gupta H V. 2007. Do Nash values have value? *Hydrological Processes* **21**: 2075–2080 DOI:
1225 10.1002/hyp

1226 Schaefli B, Hingray B, Niggli M, Musy A. 2005. A conceptual glacio-hydrological model for high
1227 mountainous catchments. *Hydrology and Earth System Sciences* **9**:95-109 DOI: 10.5194/hessd-2-
1228 73-2005

1229 Schweizer J, Kronholm K, Jamieson B, Birkeland KW. 2008. Review of spatial variability of snowpack
1230 properties and its importance for avalanche formation. *Cold Regions Science and Technology* **51** (2–
1231 3): 253–272 DOI: 10.1016/J.COLDREGIONS.2007.04.009

1232 Seibert J, Vis M, Lewis E, van Meerveld HJ. 2018. Upper and lower benchmarks in hydrological
1233 modelling. *Hydrological Processes* **32**:1120-1125 DOI: 10.1002/hyp.11476

1234 Sen PK. 1968. Estimates of the regression coefficient based on Kendall’s Tau. *Journal of the American*
1235 *Statistical Association* **63** (324): 1379–1389 DOI: 10.1080/01621459.1968.10480934

1236 Seneviratne SI, Nicholls N, Easterling D, Goodess CM, Kanae S, Kossin J, Luo Y, Marengo J, McInnes K,
1237 Rahimi M, et al. 2012. Changes in climate extremes and their impacts on the natural physical
1238 environment. In: *Managing the Risks of Extreme Events and Disasters to Advance Climate Change*
1239 *Adaptation*. Cambridge University Press.

1240 Sentlinger G, Fraser J, Baddock E. 2019. Salt Dilution Flow Measurement: Automation and Uncertainty.
1241 In *HydroSenSoft, International Symposium and Exhibition on Hydro-Environment Sensors and*
1242 *Software*. Madrid; 8. Available at: [http://www.fathomsscientific.com/wp-](http://www.fathomsscientific.com/wp-content/uploads/2018/12/HydroSense_AutoSalt_2019_V0.6.pdf)
1243 [content/uploads/2018/12/HydroSense_AutoSalt_2019_V0.6.pdf](http://www.fathomsscientific.com/wp-content/uploads/2018/12/HydroSense_AutoSalt_2019_V0.6.pdf)

1244 Shannon S, Smith R, Wiltshire A, Payne T, Huss M, Betts R, Caesar J, Koutroulis A, Jones D, Harrison S.
1245 2019. Global glacier volume projections under high-end climate change scenarios. *Cryosphere* **13**
1246 (1): 325–350 DOI: 10.5194/TC-13-325-2019

1247 Shea JM, Immerzeel WW, Wagnon P, Vincent C, Bajracharya S. 2015. Modelling glacier change in the
1248 Everest region, Nepal Himalaya. *The Cryosphere* **9** (3): 1105–1128 DOI: 10.5194/tc-9-1105-2015

1249 Stahl K, Moore RD. 2006. Influence of watershed glacier coverage on summer streamflow in British
1250 Columbia, Canada. *Water Resources Research* **42** (6) DOI: 10.1029/2006WR005022

1251 Stahl K, Moore RD, Shea JM, Hutchinson D, Cannon AJ. 2008. Coupled modelling of glacier and
1252 streamflow response to future climate scenarios. *Water Resources Research*, 44(2), 1–13.
1253 <https://doi.org/10.1029/2007WR005956>

1254 van Tiel M, Kohn I, Van Loon AF, Stahl K. 2020a. The compensating effect of glaciers: Characterizing the
1255 relation between interannual streamflow variability and glacier cover. *Hydrological Processes* **34**
1256 (3): 553–568 DOI: 10.1002/hyp.13603

1257 van Tiel M, Van Loon AF, Seibert J, Stahl K. 2021. Hydrological response to warm and dry weather: do
1258 glaciers compensate? *Hydrology and Earth System Sciences* **25** (6): 3245–3265 DOI: 10.5194/hess-
1259 25-3245-2021

1260 van Tiel M, Stahl K, Freudiger D, Seibert J. 2020b. Glacio-hydrological model calibration and evaluation.
1261 *Wiley Interdisciplinary Reviews: Water* **7** (6) DOI: 10.1002/wat2.1483

1262 Verbunt M, Gurtz J, Jasper K, Lang H, Warmerdam P, Zappa M. 2003. The hydrological role of snow and
1263 glaciers in alpine river basins and their distributed modeling. *Journal of Hydrology* **282** (1–4): 36–55
1264 DOI: 10.1016/S0022-1694(03)00251-8

1265 Walmsley JL, Taylor PA, Keith T. 1986. A simple model of neutrally stratified boundary-layer flow over
1266 complex terrain with surface roughness modulations (MS3DJH/3R). *Boundary-Layer Meteorology*
1267 **36** (1–2): 157–186 DOI: 10.1007/BF00117466

1268 Wheeler HS, Pomeroy JW, Pietroniro A, Davison B, Elshamy M, Yassin F, Rokaya P, Fayad A, Tesemma Z,
1269 Princz D, et al. 2022. Advances in modelling large river basins in cold regions with Modélisation
1270 Environnementale Communautaire—Surface and Hydrology (MESH), the Canadian hydrological land
1271 surface scheme. *Hydrological Processes* **36** (4): e14557 DOI: 10.1002/HYP.14557

1272 WMO. 1986. Intercomparison of models of snowmelt runoff. *Operational Hydrology Report No. 23*.
1273 Secretariat of the World Meteorological Organization, Geneva, Switzerland

1274 Young GJ. 1977. Relations between mass-balance and meteorological variables. *Zeitschrift für*
1275 *Gletscherkunde und Glazialgeologie* **13** (1/2): 111–125

1276 Zhou J, Pomeroy JW, Zhang W, Cheng G, Wang G, Chen C. 2014. Simulating cold regions hydrological
1277 processes using a modular model in the west of China. *Journal of Hydrology* **509**: 13–24 DOI:
1278 10.1016/J.JHYDROL.2013.11.013
1279